# Solution, Solid, and Gas Phase Studies on a Nickel Dithiolene System: Spectator Metal and Reactor Ligand

Benjamin Mogesa,[†] Eranda Perera,[†] Hannah M. Rhoda,[‡] John K. Gibson,[§] Jos Oomens,[∥] Giel Berden,[∥] Michael J. van Stipdonk,*[,†] Victor N. Nemykin,*[,‡] and Partha Basu*[,†]

[†]Department of Chemistry and Biochemistry, Duquesne University, Pittsburgh, Pennsylvania 15282, United States

[‡]Department of Chemistry and Biochemistry, University of Minnesota—Duluth, Duluth, Minnesota 55812, United States

[§]Chemical Sciences Division, Lawrence Berkeley National Laboratory, 1 Cyclotron Road, Berkeley, California 94720, United States

[∥]Radboud University, Institute for Molecules and Materials, FELIX Laboratory, Toernooiveld 7c, 6525ED Nijmegen, The Netherlands

S *Supporting Information*

ABSTRACT: The syntheses of cationic nickel complexes using N,N'-dimethyl piperazine 2,3-dithione (Me_2Dt^0) and N,N'-diisopropyl piperazine 2,3-dithione ($^iPr_2Dt^0$) ligands are reported. These ligands were used in synthesizing bis and tris(dithione)Ni(II) complexes as tetrafluoroborate or hexafluorophosphate salts, i.e., $[Ni(^iPr_2Dt^0)_2][BF_4]_2$ ($[\mathbf{1a}][BF_4]_2$), $[Ni(^iPr_2Dt^0)_2][PF_6]_2$ ($[\mathbf{1a}][PF_6]_2$), $[Ni(Me_2Dt^0)_2][BF_4]_2$ ($[\mathbf{1b}][BF_4]_2$), $[Ni(^iPr_2Dt^0)_3][BF_4]_2$ ($[\mathbf{2a}][BF_4]_2$), and $[Ni(^iPr_2Dt^0)_3][PF_6]_2$ ($[\mathbf{2a}][PF_6]_2$), respectively. Complex $[\mathbf{2a}][PF_6]_2$ was isolated from a methanolic solution of $[\mathbf{1a}][PF_6]_2$. Compound $[\mathbf{1a}][BF_4]_2$ crystallizes in a trigonal crystal system (space group, $P3_1/c$) and exhibits unique packing features, whereas $[\mathbf{2a}][BF_4]_2$ crystallizes in a monoclinic ($P2_1/n$) space group. Cyclic voltammograms of $[\mathbf{1a}][BF_4]_2$ and $[\mathbf{1b}][BF_4]_2$ are indicative of four reduction processes associated with stepwise single-electron reduction of the ligands. Spectroelectrochemical experiments on $[\mathbf{1a}][BF_4]_2$ exhibit an intervalence charge transfer (IVCT) transition as a spectroscopic signature of the mixed-valence $[Ni(^iPr_2Dt^0)(^iPr_2Dt^{1-})]^-$ species. Analysis of this IVCT band suggests that this ligand based mixed valence complex, $[Ni(^iPr_2Dt^0)(^iPr_2Dt^{1-})]^-$, behaves more like a traditional class II/III metal based mixed-valence complex. The density functional theory (DFT) and time dependent DFT calculations provide a theoretical framework for understanding the electronic structures and the nature of excited states of the target compounds that are consistent with their spectroscopic and redox properties. Vibrational spectra of $[\mathbf{1a}]^{2+}$ and $[\mathbf{2a}]^{2+}$ were investigated as discrete species in the gas phase using infrared multiple photon dissociation (IRMPD) spectroscopy.
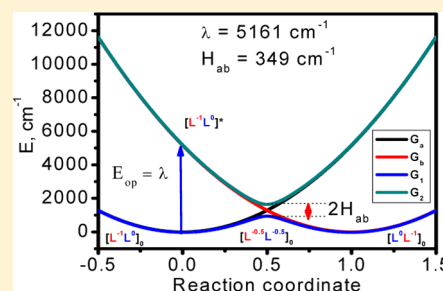
INTRODUCTION

The ene-dithiolate (or dithiolene) complexes of nickel have garnered much attention since the initial reports due to their intrinsic electronic structures that lead to extraordinary physicochemical properties.[1−3] Photophysical properties such as intense low energy charge transfer transitions led to their use as dyes[4,5] and in Q-switches.[6] In addition, these complexes exhibit high thermal and photochemical stability[7] and metallic conductivity.[8] A hallmark of the system is the efficient electronic delocalization that extends to the ligand backbone. Their ability to stabilize multiple redox states is an intriguing feature. These properties have been used in developing liquid crystalline materials with nonlinear optical properties.[4,5,9−17] In general the Ni(II)−dithiolene d[8] complexes are planar with S−Ni−S angles nearly 90°.[4] This geometric feature has been exploited in designing planar nanosheet materials reminiscent of graphene.[18] The dithiolene complexes of nickel have been used in purification of olefins[5,19,20] and in developing magnetic materials[21,22] and sensors.[23,24]

Spectroscopic and computational studies have consistently pointed out a high degree of covalency in Ni−S bonds leading to a large sulfur contribution to the highest occupied molecular orbital (HOMO). This feature also suggests that oxidation of such a center would remove electron(s) from a primarily ligand based orbital, and is consistent with the redox noninnocence nature of the dithiolene ligands.[25−27] Ligand based oxidation by one electron leads to a semioxidized (radical) ligand while oxidation by two electrons leads to a fully oxidized neutral dithione ligand. Square planar complexes of group 10 metal ions such as Ni(II), Pd(II), and Pt(II) of neutral dithione ligands have been reported.[9,28,29]

For some time, we have been interested in understanding the fundamental aspects of the metal−ligand redox interplay in transition metal dithiolene complexes (Chart 1) using both reduced[30] and oxidized ligands.[31−33] In contrast, a majority of the studies in exploring the redox noninnocence in metal−

Chart 1. Schematic Representation of Metal−Ligand Redox Interplay in bis(dithione)Ni(II) Dithiolene Complexes[a]
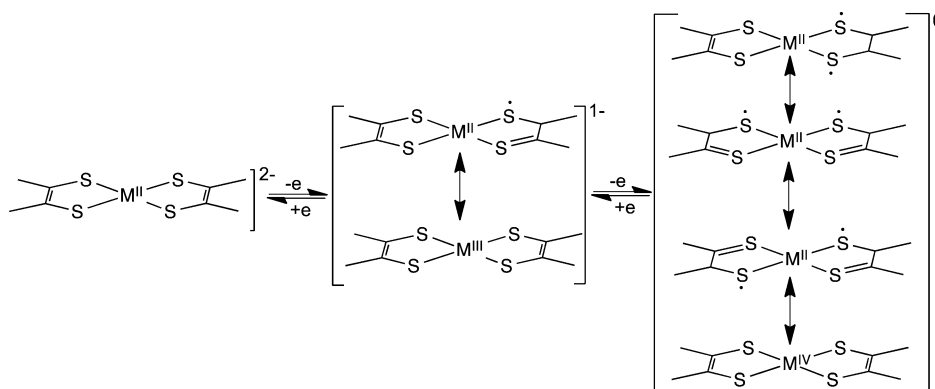
[a]Only two redox processes are shown. The odd electrons are shown with a dot.

dithiolene systems have focused on the reduced state of the ligand.[1−3] It has been reported that oxidation removes electrons from the reduced ligands, demonstrating the noninnocent nature of the ligands.[34−38] In our initial work with a fully oxidized dithiolene, i.e., dithione ligand, we observed a negative solvatochromism in a molybdenum(0) dithione complex.[33] The same dithione ligand was used in stabilizing oxo−Mo(IV) centers, and one of these complexes exhibited unique reactivity resulting in a multinuclear complex with strong metal−metal interaction.[31] More recently, we have described the ground state electronic structure of the dithione ligand as an admixture of dizwitterionic and fully oxidized forms.[32] Herein we describe syntheses, characterization, and spectroscopic and redox properties of bis(dithione)Ni(II) complexes that exhibit clean one-electron redox couples, and lower energy charge transfer transitions. Density functional calculations show that the highest occupied orbitals are predominantly metal centered while the lowest unoccupied orbitals are ligand based. This electronic description is consistent with the metal to ligand charge transfer transition observed at a lower energy as well as ligand centered redox couples. Through spectroelectrochemistry we also observed mixed valence complexes where the two dithione ligands are at different redox states.

In addition to characterizing the complexes in solid and solution phase, we have also investigated the vibrational structures in the gas phase, providing information about the intrinsic features in the absence of any condensed phase effect, which are more reliably compared to results from high-level quantum-chemical calculations. Recently, we reported gas phase vibrational structure in an oxo−molybdenum dithiolene complex, using wavelength selective infrared multiple photon dissociation (IRMPD) spectroscopy.[39] In this approach infrared spectra of gas phase species are collected via mass selection through tandem mass spectrometry in combination with a tunable mid-IR free electron laser (FEL). In IRMPD spectroscopy, absorption occurs when the FEL photon frequency matches that of a vibrational transition. Absorption of multiple photons raises the vibrational energy of the trapped ion to the dissociation threshold, and an IR *action* spectrum is generated by measuring the fragmentation induced by this process as a function of photon frequency. Vibrational mode assignment and structural determination are made with the assistance of vibrational frequencies predicted by density functional theory (DFT) or related computational methods.

■ EXPERIMENTAL SECTION

Syntheses of the nickel complexes were carried out under a dry argon or dinitrogen atmosphere using standard Schlenk techniques. The ligands, N,N'-dimethyl piperazine 2,3-dithione (Me_2Dt^0) and N,N'-diisopropyl piperazine 2,3-dithione ($^iPr_2Dt^0$), were synthesized in air according to literature procedures.[40] Solvents were purchased from either Aldrich or ACROS Organics and purified by distillation as follows: acetonitrile from CaH_2 and P_2O_5; CH_2Cl_2 and $CHCl_3$ from CaH_2; diethyl ether and toluene from sodium benzophenone; anhydrous methanol was obtained by drying over activated Mg. $NiCl_2\cdot6H_2O$ was purchased from Aldrich and used as received.

Mass spectra were collected in both negative and positive ion mode on a Waters Micromass ZMD quadrupole mass spectrometer equipped with an electrospray ionization (ESI) source, using acetonitrile as the spray solvent. Capillary voltage was kept at 3.5 kV. Dry nitrogen was used as the drying gas. Source temperature and the dissolving temperature were set at 100 and 150 °C respectively (spray rate, 150 μL/min). Additional ESI and tandem mass spectrometry experiments were conducted using a ThermoScientific (San Jose, CA) LTQ-XL LIT mass spectrometer equipped with an Ion Max ESI source. For the ESI experiments, stock solutions (0.1 mM) of the Ni-dithione samples were prepared in acetonitrile. The solution was infused into the ESI-MS instrument using the incorporated syringe pump at a flow rate of 10−15 μL/min. The atmospheric pressure ionization stack settings for the LTQ (lens voltages, quadrupole and octopole voltage offsets, etc.) were optimized for maximum transmission of the doubly charged ions to the ion trap mass analyzer by using the autotune routine within the LTQ Tune program. Helium was used as the bath/buffer gas to improve trapping efficiency and as the collision gas for CID experiments.

For CID, precursor ions were isolated using an isolation width of 1.0 to 2.5 mass-to-charge (m/z) units. The exact value was determined empirically to provide maximum isolated ion intensity while ensuring isolation of a single isotopic peak. The normalized collision energy (NCE, as defined by ThermoScientific) was set between 5 and 18%, which corresponds to the application of roughly 0.55−0.68 V tickle voltage to the end-cap electrodes with the current instrument calibration. The activation Q, which defines the frequency of the applied rf potential, was set at 0.30. In all cases, the activation time employed was 30 ms. Spectra displayed represent the accumulation and averaging of at least 30 isolation, dissociation, and ejection/detection steps.

UV−visible spectra were recorded on a modified temperature-controlled Cary 14 spectrophotometer. All ^1H and ^{13}C NMR spectra were recorded on either a Bruker 500 MHz or a 400 MHz spectrometer. The FTIR spectra of neat samples were recorded on a Thermo Electron corporation Nicolet 380 spectrometer. Elemental analysis was performed at Midwest Microlab LLC, Indianapolis, IN. Electrochemical measurements were conducted on a Bioanalytical Systems (BAS) model CV-50W electrochemical analyzer. Voltammo-

grams were recorded at 25 °C with a standard three-electrode system consisting of a platinum working electrode, a Ag^+/Ag reference electrode, and a Pt-wire auxiliary electrode. All voltammograms were internally referenced with ferrocenium/ferrocene couple. Either tetraethylammonium perchlorate, tetraethylammonium tetrafluoroborate, or tetraethylammonium hexafluorophosphate were used as the supporting electrolytes.

Spectroelectrochemical data were collected on a JASCO-720 spectrophotometer at room temperature, and the experiments were conducted using a CHI-620C electrochemical analyzer using a custom-made 1 mm cell, and a Pt mesh-working electrode. Measurements were conducted in 0.30 M solutions of TBAP in CH_3CN or CD_3CN to suppress solvent overtones in the NIR region of the optical spectra. Because of the relatively low solubility of $[1b][BF_4]_2$, in acetonitrile, all spectroelectrochemical experiments were conducted with $[1a][PF_6]_2$.

X-ray Structure Determination. Suitable single crystals were coated with Paratone and mounted on a glass fiber, and the data were collected using a Bruker SMART Apex II diffractometer with a graphite monochromator for Mo Kα radiation (0.71073 Å). The absorption correction was performed using SADABS routine.[41,42] The structure solution and the refinement were done using SHELXS-97 and SHEXLX-97 programs.[42] Data were collected at 296 K, and crystallographic data are listed in Table 1. All non-hydrogen atoms were refined anisotropically, and hydrogen atoms were placed at calculated positions and refined with isotropic displacement parameters.

Table 1. Crystal Data for $[1a][BF_4]_2$ and $[2a][BF_4]_2$

	$[1a][BF_4]_2$	$[2a][BF_4]_2$
empirical formula	$C_{20}H_{36}B_2F_8N_4NiS_4$	$C_{30}H_{54}B_2F_8N_6NiS_6$
formula wt	693	923
temp, K	296(2)	296(2)
cryst syst	monoclinic	trigonal
space group	$P2_1/n$	$P3_1/c$
cryst dimens, mm	0.050 × 0.250 × 0.630	0.11 × 0.17 × 0.60
unit cell dimens		
a, Å	6.3719(6)	15.0044(11)
b, Å	13.1449(12)	15.0044(11)
c, Å	18.4581(17)	11.995(2)
α, deg	90	90
β, deg	96.073(7)	90
γ, deg	90	120
vol, Å^3	1537.3 (2)	2338.7 (5)
Z	2	1
no. of data/params	3404/182	1743/83
data > $2\sigma(I)$	1807	1200
final R indices	R1 = 0.0627	R1 = 0.0640
$I > 2\sigma(I)$	wR2 = 0.1977	wR2 = 0.2364
R(int)	0.0957	0.0716
goodness-of-fit	1.007	1.050

ESI FT-ICR Mass Spectrometry. A stock solution ($\sim1.0 \times 10^{-4}$ molar) of $[1a][BF_4]_2$ was prepared in acetonitrile for the IRMPD experiments. Previously established methods used by our group for generation of ions and the subsequent collection of IRMPD spectra[43–48] were used here. Briefly, ESI was performed using a Micromass (now a component of Waters Corporation, Milford MA) Z-Spray source. Dry nitrogen (~80 °C) was used to assist in the desolvation process. Ions were injected into a home-built Fourier transform ion cyclotron resonance (FT-ICR) mass spectrometer described in detail elsewhere.[49] Ions were accumulated for the duration of the previous FT-ICR cycle (4.5 s) in a linear hexapole trap and injected into the ICR cell via a quadrupole deflector and an octopole RF ion guide. ESI of the acetonitrile solution of $[1a][BF_4]_2$ produced an intense ion with m/z values of 259 and 260, corresponding to the bis(dithione)Ni(II) complex, $^{58}Ni(^iPr_2Dt^0)_2^{2+}$

and $^{60}Ni(^iPr_2Dt^0)_2^{2+}$. A less abundant species with m/z values of 374 and 375 was also observed. These peaks were assigned to the tris(dithione)Ni(II) complex, $^{58}Ni(^iPr_2Dt^0)_3^{2+}$ and $^{60}Ni(^iPr_2Dt^0)_3^{2+}$. Instrument operating parameters, such as desolvation temperature, cone voltage, and ion accumulation and transfer optics voltages, were optimized to maximize the intensity of either the bis or the tris(dithione)Ni(II) complexes in the ICR cell. Mass isolation of a single species was achieved using stored waveform inverse Fourier transform (SWIFT) techniques prior to irradiation by the FEL.

Infrared Multiple Photon Dissociation (IRMPD). Infrared spectra were recorded by measuring the photodissociation yield as a function of photon frequency. Precursor anions were irradiated for 2.5 s using 12 FELIX macropulses (35–50 mJ per macropulse, 5 μs pulse duration, fwhm bandwidth ~0.5% of central λ). In the IRMPD process, a photon is absorbed when the laser frequency matches that of an IR active vibrational mode of the gas phase ion and its energy is subsequently distributed over all vibrational modes by intramolecular vibrational redistribution (IVR). The IVR process allows the energy of each photon to be dissipated before the ion absorbs another, which leads to promotion of the ion's internal energy toward the dissociation threshold via multiple photon absorption.[50] It is important to note that infrared spectra obtained using IRMPD are usually comparable to those collected using linear absorption techniques.[49,51] For these experiments, the FEL wavelength was tuned between 900 and 1800 cm^{-1} (5.5 and 11 μm) in 6 cm^{-1} increments. The intensities of product and undissociated precursor ions were obtained from an averaged mass spectrum measured using the excite/detect sequence of the FT-ICR-MS after each IRMPD step. The IRMPD yield was normalized to the total ion current and linearly normalized for variations in the laser intensity.

Computational Details. All DFT calculations were performed using Gaussian 09.[52] Molecular orbital contributions were compiled from single point calculations using the VMOdes program.[53] In order to investigate the nature of the excited states in bis and tris(dithione)-Ni(II) complexes, pure GGA BP86,[54,55] hybrid (10% of Hartree−Fock exchange) TPSSh,[56] and hybrid (20% of Hartree−Fock exchange) B3LYP[57] were used. It has been reported that in these complexes the energies of excited states have strong dependency on the amount of Hartree−Fock exchange present in exchange-correlation functional.[58] It was found (Figure S4) that B3LYP exchange-correlation functional provides the best agreement between theory and experiment, and thus, only data on these calculations are discussed below.[30] Wachter's full-electron basis set was used for nickel,[59] while for all other atoms 6-311G(d) basis set[60] was employed. Geometries of Ni-containing cations, $[1a]^{2+}$ and $[2a]^{2+}$, were fully optimized without any restrictions or substituent truncations. In the case of $[1a]^{2+}$, the highest point group (taking into consideration the nonplanar nature of the dithione ligand) was found to be C_{2h}, while in the case of $[2a]^{2+}$, the molecular point group was found to be close, but not exactly at D_3 symmetry. In both cases, no imaginary frequencies were found after complete optimizations thus ensuring the potential energy minima. In order to cover its experimental UV−visible spectrum of $[1a][BF_4]_2$ and $[2a][PF_6]_2$, the first 50 excited states were considered in TDDFT calculations. The solvent effects were modeled using the PCM approach[61] implemented into the Gaussian 09 program. For IRMPD calculations, initial optimization of $[1a]^{2+}$ was performed at the B3LYP/3-21G* level of theory using geometries in which dithione ligands were randomly arranged around the Ni^{2+}. Several minima were identified after the initial calculations, which differed only in the orientation of the isopropyl group with respect to the ring. The lowest energy structure was subjected to full optimization using the same functional and the 6-311+G(d) basis set on atoms. Vibrational frequencies for comparison to IRMPD spectra, calculated at the same level of theory, were scaled by factors of 0.97 and 0.95 (chosen empirically) for the bis and tris(dithione)Ni(II) complexes, respectively, to facilitate peak assignment.

Synthetic Details. *Synthesis of $[Ni(^iPr_2Dt^0)_2][BF_4]_2$ ($[1a][BF_4]_2$).* 130 mg (0.547 mmol) of $NiCl_2\cdot6H_2O$ was added to a Schlenk flask filled with 10 mL of methanol. After stirring for a few minutes, 250 mg (1.085 mmol) of $^iPr_2Dt^0$ ligand was added to the reaction mixture. The

green solution turned blue when an excess (1:10) of $NaBF_4$ was added, precipitating the target complex. The precipitate was washed with water to dissolve excess $NaBF_4$ and was recrystallized from acetonitrile−ether to obtain analytically pure compound. Yield: 250 mg, 66% (0.366 mmol). Anal. Calcd (experimental) for $C_{20}H_{36}N_4S_4NiB_2F_8H_2O$: C, 33.78 (33.55); H, 5.39(5.07); N, 7.88(7.82). ^{1}H NMR (CD_3CN) δ, ppm: 5.13 (CH, 2H, sep, 7.1 Hz), 3.89 (CH_2, 4H, s). 1.39 (CH_3, 12H, d, 7.1 Hz). ^{13}C NMR (CD_3CN) δ: 181.96 (C=S), 59.87 (CH), 42.06 (CH_2), 16.64 (CH_3). FTIR (neat, cm^{-1}): 1535 (vs, C−N), 1368 (vs, C=S), 1395 (vs), 1286 (s), 1051 (vs, BF_4), 1019 (s). ESI-MS (MeCN): m/z 518[M]$^+$. UV−vis, λ_{max} (CH_3CN, ε, M^{-1} cm^{-1}): 604 (5690), 540 (4830), 317 (37640).

Synthesis of [Ni($^iPr_2Dt^0$)$_2$][PF$_6$]$_2$ ([1a][PF$_6$]$_2$). In a Schlenk flask, 100 mg (0.42 mmol) of $NiCl_2·6H_2O$ was dissolved in 15 mL of methanol. The solution was stirred for 10 min, after which 180 mg (1.05 mmol) of $^iPr_2Dt^0$ ligand was added. The green reaction mixture turned blue upon addition of a slight excess (1:2.5) of $NaPF_6$, and the target complex precipitated. The precipitate was filtered, washed with methanol (1 mL × 3) to remove excess $NaPF_6$, and dried in vacuum to obtain analytically pure compound. Yield: 160 mg, 47% (0.198 mmol). Anal. Calcd (experimental) for $C_{20}H_{36}N_4S_4NiP_2F_{12}$: C, 29.68(29.44); H, 4.48(4.41); N, 6.92(6.87). ^{1}H NMR (CD_3CN) δ, ppm: 5.11 (CH, 2H, m), 3.86 (CH_2, 4H, s). 1.39 (CH_3, 12H, d). ^{13}C NMR (CD_3CN) δ: 181.71 (C=S), 60.05 (CH), 41.88 (CH_2), 17.06 (CH_3). FTIR (neat, cm^{-1}): 1530 (vs, C−N), 1368 (vs, C=S), 827 (vs, PF_6). UV−vis, λ_{max} (CH_3CN, ε, M^{-1} cm^{-1}): 610 (5780), 542 (4820), 322 (35040).

Synthesis of [Ni(Me$_2$Dt^0)$_2$][BF$_4$]$_2$ ([1b][BF$_4$]$_2$). The procedure was slightly different from the synthesis of [Ni($^iPr_2Dt^0$)$_2$][BF$_4$]$_2$. 170 mg (0.715 mmol) of $NiCl_2·6H_2O$ was added to a Schlenk flask filled with 15 mL of acetonitrile. After stirring for few minutes, 250 mg (1.434 mmol) of Me_2Dt^0 ligand was added to the reaction mixture. The green solution turned blue when an excess (1:10) of $NaBF_4$ was added, and a blue colored solid precipitated. The precipitate was washed with water to eliminate excess $NaBF_4$ and was recrystallized from acetonitrile−ether to get analytically pure target compound. Yield: 265 mg, 64% (0.460 mmol). Anal. Calcd (experimental) for $C_{12}H_{20}N_4S_4NiB_2F_8·CH_3CN$: C, 27.04 (27.05); H, 3.73 (3.80); N, 11.26 (10.16). FTIR (neat, cm^{-1}): ^{1}H NMR (CD_3CN) δ: 4.03 (CH_3, 6H, s), 3.91 (CH_2, s, 4H). ^{13}C NMR (CD_3CN) δ: 179.19 (C=S), 49.82 (CH_2), 46.06 (CH_3). 1572 (vs, C−N), 1372 (vs, C=S), 1395 (vs), 1270 (s), 1049 (vs, BF_4), 1015 (s). ESI-MS (MeCN): m/z 406[M]$^+$, 203 [M]$^{2+}$. UV−vis λ_{max} (CH_3CN, ε, M^{-1} cm^{-1}): λ_{max} (CH_3CN, M^{-1} cm^{-1}): 604 (4200), 540 (4022), 317 (39570).

Synthesis of [Ni($^iPr_2Dt^0$)$_3$][PF$_6$]$_2$ ([2a][PF$_6$]$_2$). This complex was isolated from a methanolic solution of [Ni($^iPr_2Dt^0$)$_2$][PF$_6$]$_2$ ([1a]-[PF$_6$]$_2$). In a 20 mL vial, 0.06 g of [1a][PF$_6$]$_2$ was dissolved in 20 mL of methanol, and in another 20 mL vial, 0.05 g of the same compound was dissolved in methanol and was layered with acetone. The two solutions were left standing, in air, for 2 days, after which a green precipitate formed. The precipitate was filtered and dried in vacuum. A total of 0.025 g of product was collected (4% yield). Anal. Calcd (experimental) for $C_{30}H_{54}N_6S_6NiP_2F_{12}$: 34.65(34.78); 8.08(7.94); 5.23(5.11). FTIR (neat, cm^{-1}): 1503 (vs, C−N), 1364 (vs, C=S), 1282 (vs), 1258 (s), 829(vs, PF_6). UV−vis, λ_{max} (CH_3CN−DMF: 60:40; ε, M^{-1} cm^{-1}): 315 (36674); 413 (4674); 750 (337). ^{1}H NMR (CD_3CN−DMF-d_7 (6:4)) δ: 1.27 (CH_3, broad, 12H), 3.28 (CH_2, broad, 2H), 6.68 (CH_2, broad, 2H), 15.58 (CH, broad, 2H). The molar extinction coefficients were calculated by correcting for the presence of [1a][PF$_6$]$_2$ in solution as evidenced from the band ∼615 nm (∼8%).

■ RESULTS AND DISCUSSION

Syntheses and Characterization. The nickel complexes were synthesized by reacting the neutral dithione ligand with a methanolic solution of $NiCl_2·6H_2O$. The complexes are formed presumably due to the chelate effect of the ligand. The cationic complexes [1a]$^{2+}$ and [1b]$^{2+}$ precipitated as boron tetrafluoride or hexafluorophosphate salts in the presence of an excess of $NaBF_4$ or $NaPF_6$, respectively. The ^{13}C NMR spectra for complexes [1a][BF$_4$]$_2$ and [1b][BF$_4$]$_2$ exhibit a C=S peak at δ 182 and 179 respectively, which are close to the peaks observed in the free ligands, δ 181 and 180 respectively. This is an indication that in solution the coordinated ligands are still in the fully oxidized state. A similar conclusion can be reached from the IR spectra in the solid state, the C=S stretching frequencies observed at 1368 cm^{-1} and at 1372 cm^{-1} for [1a][BF$_4$]$_2$ and [1b][BF$_4$]$_2$, respectively. Both [1a][BF$_4$]$_2$ and [1b][BF$_4$]$_2$ are 1:2 electrolyte and are diamagnetic. The molecular nature of all complexes was further confirmed by electrospray ionization mass spectrometry (ESI-MS). The characteristic molecular ion peak for [1a]$^{2+}$ was observed at 259 m/z for [M]$^{2+}$. It was interesting to note that, at 3.5 V cone voltage (normal cone is set at 3.0 V), a peak was observed at 518 m/z for the [M]$^+$ peak. It was similar for [1b]$^{2+}$, where the molecular ion peaks were observed at 406 m/z (minor) for [M]$^+$ and at 203 for [M]$^{2+}$.

Compound [2a][PF$_6$]$_2$ was isolated from methanolic solutions of [1a][PF$_6$]$_2$ in low yields. Direct synthesis of this complex by increasing the metal:ligand ratio was unsuccessful, as the bis(dithione)Ni(II) complex precipitated from the reaction mixture. Complex [2a][PF$_6$]$_2$ is insoluble in pure methanol and sparingly soluble in acetonitrile, but is soluble in DMF, resulting in a green solution. However, the DMF solution degrades rapidly. Conversion of [1a][PF$_6$]$_2$ to [2a][PF$_6$]$_2$ was probed in solution by UV−visible spectroscopy in a mixture of acetonitrile and DMF. Increasing the fraction of DMF with respect to acetonitrile results in degradation of [1a][PF$_6$]$_2$ and formation of [2a][PF$_6$]$_2$, as the solution turns from blue to green. A 3:2 acetonitrile:DMF solvent mixture was found be a reasonable compromise. The ^{1}H NMR spectra taken in this solvent mixture exhibited several paramagnetically shifted resonances confirming the paramagnetic nature of this complex. Conversion of [1a][PF$_6$]$_2$ to [2a][PF$_6$]$_2$ is irreversible; similar experiments with [2a][PF$_6$]$_2$ did not yield any detectable [1a][PF$_6$]$_2$. The mass spectra of [1a][PF$_6$]$_2$ taken in acetonitrile solutions also show the presence of both [1a]$^{2+}$ and [2a]$^{2+}$ although [1a]$^{2+}$ at a higher proportion. The ESI-MS of acetonitrile:DMF solutions of analytically pure [2a][PF$_6$]$_2$ also shows molecular ion peaks due to [1a]$^{2+}$ and [2a]$^{2+}$ with peaks due to [2a]$^{2+}$ at a higher proportion, along with free ligand and several unidentified peaks. This experiment suggests that, under these experimental conditions, [2a][PF$_6$]$_2$ is degraded and a small amount of [1a]$^{2+}$ is formed, which was not detectable by UV−visible spectroscopy. The solid state IR spectrum of [2a][PF$_6$]$_2$ exhibits a vibration at 1364 cm^{-1} due to the C=S stretch. A strong stretch due to PF_6 was also observed at ∼830 cm^{-1}.

Molecular Structures. Compound [1a][BF$_4$]$_2$ was crystallized by slow evaporation of either acetonitrile/ether or methanol/ether solutions. In acetonitrile, green needle-shaped crystals were obtained while crystals from methanol/ether appeared reddish green in color. Both crystals were characterized by single crystal X-ray structure diffractometry, and relevant data are presented in Table 1. Crystals obtained from methanol/ether yielded a tris(dithione)Ni(II) complex, [2a][BF$_4$]$_2$. Compound [1a][BF$_4$]$_2$ crystallizes in the monoclinic crystal system, with space group $P2_1/n$, whereas [2a][BF$_4$]$_2$ crystallized in trigonal crystal system, with space group $P3_1/c$. Selected bond distances and bond angles are shown in Table 2, whereas the molecular structures are shown

Table 2. Selected Bond Lengths and Angles of [1a][BF₄]₂ and [2a][BF₄]₂

[1a][BF₄]₂				[2a][BF₄]₂			
bond length, Å		bond angle, deg		bond length, Å		bond angle, deg	
Ni1−S1	2.160(2)	S1−Ni1−S2	91.46(6)	Ni(1)−S(2)	2.3785(11)	S2−Ni1−S2	93.66(5)
Ni1−S2	2.167(2)	C1−S1−Ni1	105.6(2)	S(2)−C(1)	1.676(4)	S2−Ni1−S2	86.17(4)
S2−C2	1.694(4)	C2−S2−Ni1	105.1(2)	C(3)−C(5)	1.494(8)	C1−S2−Ni1	105.20(12)
S1−C1	1.699(5)	N1−C1−S1	122.0(4)	C(3)−N(1)	1.502(5)	C5−C3−N1	112.8(4)
N2−C2	1.311(6)	C2−C1−S1	118.0(4)	C(3)−C(4)	1.552(8)	C5−C3−C4	112.9(5)
N1−C1	1.315(6)	N1−C1−C2	120.0(5)	C(1)−N(1)	1.316(4)	N1−C3−C4	108.4(4)
N2−C8	1.489(7)	C1−C2−S2	117.9(3)	C(1)−C(1)	1.522(7)	N1−C1−C1	117.5(2)
N1−C5	1.502(7)	N2−C2−S2	122.4(4)	C(2)−N(1)	1.480(5)	N1−C1−S2	122.5(3)
N1−C4	1.480(6)	N2−C2−C11	119.8(4)	C(2)−C(2)	1.505(8)	C1−C1−S2	119.94(14)
C1−C2	1.491(7)						
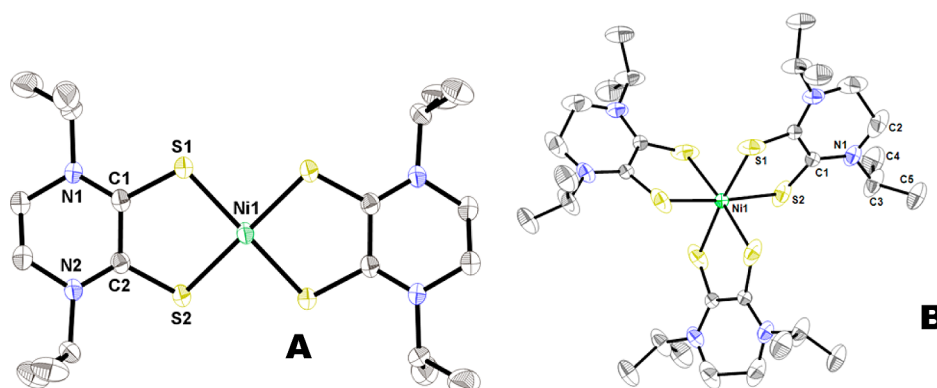
Figure 1. Molecular structure of [1a][BF₄]₂ (A) and [2a][BF₄]₂ (B) shown with 30% thermal ellipsoids; hydrogen atoms and the anions are omitted for clarity.
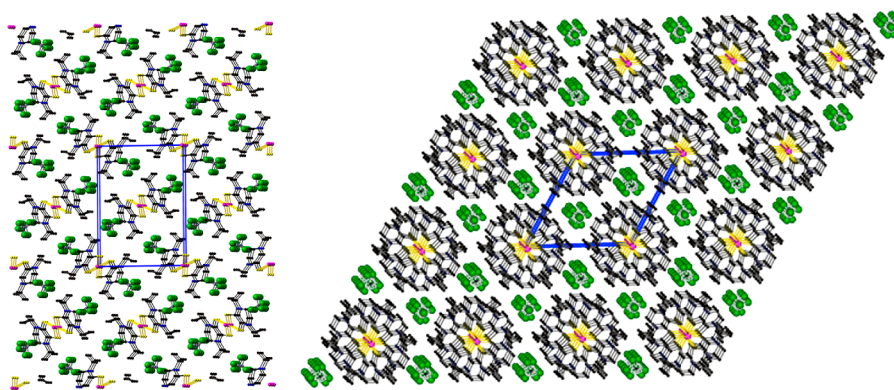
Figure 2. Packing of [1a][BF₄]₂ (left panel; viewed along the a-axis; the b-axis is pointing horizontally to the right, and the c-axis is pointing vertically down) and [2a][BF₄]₂ (right panel; viewed along the c-axis; the a-axis is pointing horizontally to the right, and the b-axis is pointing down). Hydrogen atoms are omitted for clarity. Unit cells are shown as blue boxes.

in Figure 1. The C=S and C−C bond distances in [1a][BF₄]₂ are very similar to those of the ligand, i.e., no difference in the C−C bond distance (1.49 Å) but the C=S distance increased by ~0.02 Å due to coordination to the metal. The C=S and C−C bond distances are consistent with an oxidized form of the ligand coordinated to the metal. The observed C=S and C−C distance are different from that observed for bis-(dithiolene)Ni complexes.[62−64] For instance, in [NEt₄][Ni-(mnt)₂] complex, the C−S and the C−C distances are ~1.720(7) Å and ~1.375(10) Å, respectively.[30] The S1−C1−C2−S2 torsion angle of [1a][BF₄]₂ is reduced to 13.05° from 36.87°, that of the free ligand. Also in dithiolene complexes, the Ni−S distance is shorter due to the strong metal sulfur

interactions. The d$_{xy}$ orbital overlaps more extensively with the ligand orbitals in dithiolene complexes than for dithione complexes. Bigoli and co-workers reported the crystal structure of [Ni(Me₂Dt⁰)₂][BF₄]₂[65,66] where the C=S (1.688 (8) Å) and C−C (1.477 (12) Å) bond distances are slightly shorter than those observed in [1a][BF₄]₂ (C=S, 1.694 (4) Å, and C−C, 1.492 (7)). Similar situations have been observed in Au, Pt, and Pd dithione complexes with the same ligand (Me₂Dt⁰), where the C=S and C−C bond distances were shorter than that of [1a][BF₄]₂.[29,67−71] During crystallization of [1a][BF₄]₂, suitable crystals of [2a][BF₄]₂ were obtained for structural studies.

To date, only a handful of tris Ni(II) complexes have been reported and none with a dithiolene ligand.[15,67,72−74] Therefore, the structure of [**2a**][BF$_4$]$_2$ represents a rare example. In [**2a**][BF$_4$]$_2$, the C=S bond distance (1.676 (4) Å) is slightly longer than that of the ligand but shorter than [**1a**][BF$_4$]$_2$. The C−C bond distance (1.522 (7) Å) is, however, slightly longer than that in the ligand as well as in [**1a**][BF$_4$]$_2$. The bond distances indicate that, in [**2a**][BF$_4$]$_2$, the C−C bond is indeed a single bond. When comparing the Ni−S distance of this complex with that of [**1a**][BF$_4$]$_2$, [**2a**][BF$_4$]$_2$ has a longer distance (∼0.2 Å), suggesting a steric crowding at the metal center due to the three ^{i}Pr$_2$Dt^0 ligands. The longer Ni−S distance in [**2a**][BF$_4$]$_2$ can also be attributed to the spin change as compared to complexes [**1a**][BF$_4$]$_2$. The S1−C1−C2−S2 torsion angle of the complex (23.45°) was larger than that of [**1a**][BF$_4$]$_2$ but smaller than that of the free ligand. The structure is consistent with Ni in 2+ oxidation state with d^8 configuration, although the geometry is not. The packing diagrams of the two complexes (Figure 2) show that the anions occupy the space between the cations. However, the structure of complex [**2a**][BF$_4$]$_2$ is more compact where the three ligands span like a wheel. In the case of [**1a**][BF$_4$]$_2$ the planar Ni center leaves more voids.

Electronic Spectra. A low energy band (700−1000 nm) is characteristic of the bis(dithiolene)Ni complexes where the ligand is in a fully reduced state.[75−77] In monoanionic complexes this band shifts to the near IR region. However, in cationic complexes, no bands are observed in the near IR region.[66]

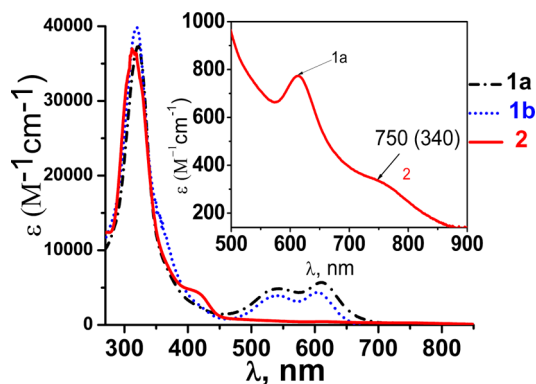The electronic spectra of complexes [**1a**][BF$_4$]$_2$ and [**1b**][BF$_4$]$_2$ are shown in Figure 3. Both complexes exhibit

Figure 3. Electronic spectra of complexes [**1a**][BF$_4$]$_2$ and [**1b**][BF$_4$]$_2$ in acetonitrile, and that of [**1a**][PF$_6$]$_2$ in acetonitrile−DMF(60:40). The inset shows the spectrum of [**2a**][PF$_6$]; the band ∼600 nm is assigned to [**1a**]$^{2+}$.

two strong low energy transitions at ∼604 nm (ε = 5690 M^{-1} cm^{-1}) and at 540 nm (ε = 4830 M^{-1} cm^{-1}), respectively, for [**1a**][BF$_4$]$_2$. The high extinction coefficients of these transitions are indicative of the charge transfer character. Similar charge transfer bands have been observed in dithiolene complexes originating from the HOMO (mixture of dithiolate, ligand π orbitals, and the metal d-orbitals) to the LUMO.[78] Such a dithiolate based π delocalized description is characteristic of metal(II) (dithiolene)$_2$ complexes. In all the complexes studied here, no transition was observed in the near-infrared region. The PF$_6$ salt, i.e., [**1a**][PF$_6$]$_2$, shows similar peak positions and molar absorptivities. On the other hand, acetonitrile−DMF

solutions of [**2a**][PF$_6$] show a relatively strong band at 413 nm (ε = 4674 M^{-1} cm^{-1}) and a weak band at 750 nm (ε = 337 M^{-1} cm^{-1}). The latter has been assigned as a predominantly d−d transition due to its low intensity.

Electrochemistry. The redox behavior of [Ni-(S$_2$C$_2$(CN)$_2$)$_2$]$^{2-}$ and related systems reported the formation of Ni(I) species upon one electron reduction of [Ni-(Dt^{2-})$_2$]$^{2-}$.[79,80] They characterized the Ni(I) species by EPR and UV−vis spectroscopy. Electrochemical behavior of nickel complexes of phenyl-substituted dithiolene, i.e., [Ni-(S$_2$C$_2$(Ph)$_2$)$_2$]$^{2-}$, exhibits two well-defined redox couples that can be attributed to oxidation and reduction of the dianion by removing or adding an electron to a highly delocalized molecular orbital.[30] In the present case, [**1a**][BF$_4$]$_2$ and [**1b**][BF$_4$]$_2$ exhibit four well-defined reversible single-electron reduction couples. No oxidative couple was observed within the electrochemical window of acetonitrile, i.e., ∼1.5 V under the experimental conditions. The cyclic voltammograms of the two complexes are shown in Figure 4, and the redox potentials are listed in Table 3.

We attribute these reduction couples to ligand-centered processes (Scheme 1). We note that the complexes were synthesized from Ni(II) salt. If the metal center was oxidized to the Ni(III) state, it would be less stable with neutral ligands coordinating the metal center. In that case, the metal center would be paramagnetic with d^7 configuration resulting in paramagnetically shifted chemical shifts in the NMR spectra, which were not observed. The DFT calculations, discussed later, suggest that the unoccupied frontier orbitals are ligand centered in nature. The electrochemical behavior indicates that both ligands are in the fully oxidized state and is consistent with the spectroscopic signatures. The electrochemistry also indicates that the ligands can be reduced reversibly at least under the cyclic voltammetric conditions, by one electron at a time (Scheme 1).

A pertinent question is how to assign these redox potentials to two redox active ligands. There are two major factors that influence redox potential of a redox active center. The first of the two is the inherent energy of the redox orbital that can be influenced by geometry as well as by the electron donating/withdrawing power of substituents attached to the molecular framework.[81] The second factor can be viewed as a perturbation that arises from the solvation of the redox center as well as specific ion-pairing.[82] The solvation components are important in the event that the redox center in the molecule is affected differently from other parts of the molecules such as in a dendrimer encapsulated redox center.[82−88] However, in the present case the solvation component is expected to be less significant in dictating the difference in the redox potentials. In order to understand the charge stabilization through ion pairing, redox potentials of [**1a**][BF$_4$]$_2$ were determined as a function of different electrolyte. Thus, three different electrolytes, i.e., ^{n}Bu$_4$NClO$_4$, Et$_4$NBF$_4$, and Et$_4$NPF$_6$, with varying size and coordination ability were tested. No significant effect on the potential was observed, indicating that, under the experimental conditions, stabilization of charge had little effect on successive electron transfer. Therefore, the difference in the electron transfer series is inherent to the molecule.

The potentials in [**1a**][BF$_4$]$_2$ are more negative than those in [**1b**][BF$_4$]$_2$, indicating that [**1a**][BF$_4$]$_2$ is more difficult to reduce. At the first approximation, this difference can be attributed to a higher electron donating ability of the isopropyl groups as compared to that of the methyl groups present in the
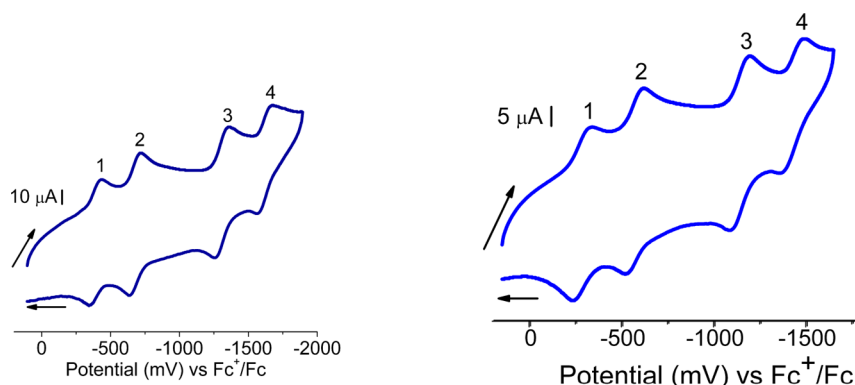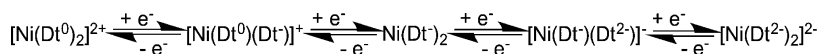
Figure 4. Cyclic voltammograms of [**1a**][BF$_4$]$_2$ (left) and [**1b**][BF$_4$]$_2$ (right). Scan rate, 100 mV s^{-1}; temperature, 25 °C ; solvent, carbon disk working electrode. Ag$^+$/Ag reference electrode, and a Pt-wire auxiliary electrode; supporting electrolyte, Et$_4$NBF$_4^-$. Potentials referenced internally with respect to Fc$^+$/Fc couple.

Table 3. Room Temperature Reduction Potentials (vs Fc$^+$/Fc) Determined in Acetonitrile

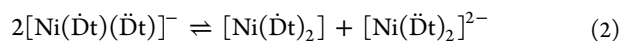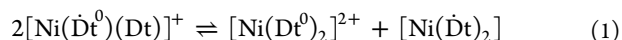|	$E_{1/2}^1$ (ΔE_p), mV	$E_{1/2}^2$ (ΔE_p), mV	$E_{1/2}^3$ (ΔE_p), mV	$E_{1/2}^4$ (ΔE_p), mV
[**1a**][BF$_4$]$_2$ (^{t}Bu$_4$NClO$_4$)	−382 (80)	−683 (73)	−1311 (105)	−1633 (95)
[**1a**][BF$_4$]$_2$ (Et$_4$NBF$_4$)	−388 (92)	−694 (82)	−1320 (100)	−1625 (75)
[**1a**][BF$_4$]$_2$ (Et$_4$NPF$_6$)	−381 (95)	−687 (85)	−1318 (96)	−1621 (83)
[**1b**][BF$_4$]$_2$ (^{t}Bu$_4$NClO$_4$)	−292 (68)	−579 (79)	−1138 (104)	−1448 (131)

Scheme 1. Ligand Centered Redox Processes Involving Fully Reduced Dithiolene (Dt^{2-}), One Electron Oxidized Dithiolene (Dt$^-$), and Fully Oxidized Dithione (Dt^0) Ligand

$$[\text{Ni}(\text{Dt}^0)_2]^{2+} \underset{-\,e^-}{\overset{+\,e^-}{\rightleftharpoons}} [\text{Ni}(\text{Dt}^0)(\text{Dt}^-)]^+ \underset{-\,e^-}{\overset{+\,e^-}{\rightleftharpoons}} \text{Ni}(\text{Dt}^-)_2 \underset{-\,e^-}{\overset{+\,e^-}{\rightleftharpoons}} [\text{Ni}(\text{Dt}^-)(\text{Dt}^{2-})]^- \underset{-\,e^-}{\overset{+\,e^-}{\rightleftharpoons}} [\text{Ni}(\text{Dt}^{2-})_2]^{2-}$$

ligand. The differences in the four redox couples (ΔE) in the two compounds are not the same; they are 90 mV, 104 mV, 173 mV, and 185 mV, respectively. The difference increases with each redox couple, i.e., addition of electrons to [**1a**][BF$_4$]$_2$ becomes progressively difficult compared to [**1b**][BF$_4$]$_2$. Addition of a second electron in [**1a**][BF$_4$]$_2$ is more difficult than adding a second electron to [**1b**][BF$_4$]$_2$. The addition of a third and a fourth electron follows the same pattern. Interestingly, $\Delta(\Delta E^1 - \Delta E^2) \approx \Delta(\Delta E^3 - \Delta E^4) \approx 13$ mV whereas $\Delta(\Delta E^2 - \Delta E^3) \approx 69$ mV (where superscripts 1–4 represent the four redox couples, see Figure 4). We infer that the addition of the third electron occurs at the ligand that has already been reduced once by one electron, which suggests that the two ligands are reduced sequentially one electron at a time, unlike one ligand being reduced fully and then the reduction of the other ligand occurs. This is also consistent with the difference in redox potentials when the same ligand is reduced, i.e., ligand 1($\Delta E^1 - \Delta E^3$) $\approx$ ligand 2 ($\Delta E^2 - \Delta E^4$) ≈ 82 mV. This aspect is summarized in Scheme 1.

Interactions between two or more redox active metal centers connected by a spacer ligand are of great interest in the context of mixed valency in molecular wires and switches.[89−94] A conceptual framework can be seen in the classic example of the Creutz−Taube ion where the two redox active metal (Ru) centers are connected by a pyrazine ligand.[95] Mixed valency in transition metal complexes, however, is more broadly defined in terms of Robin−Day classification.[96] Accordingly, three different classes of mixed valency are described: class I complexes are considered to be valence trapped, whereas class III complexes dsiplay extensive electronic delocalization between the two metal centers such that they are spectroscopically indistinguishable. Class II complexes are between classes I and III, where

there is localization of valence states with a low energy barrier. Intervalence charge transfer transition is observed in such complexes. As mentioned before, in the reduced dithiolene complexes of nickel, we[30] and others[76,97−100] have demonstrated that the frontier orbitals are dominated by sulfur character. As expected, upon addition of electrons, the ligands are reduced in the oxidized dithione complexes described here, and the metal center can be viewed as a scaffold holding the two redox active ligands even though the metal orbitals contribute to the redox orbitals. Therefore, the present case can be viewed as "role reversal" of the dinuclear mixed valence metal complex. Under this premise one can write comproportionation reactions, eqs 1 and 2, involving mixed redox states of the ligand. The comproportionation constant (K_c)[101] in each case can be calculated from the redox potentials following eq 3.

$$2[\text{Ni}(\dot{\text{Dt}}^0)(\text{Dt})]^+ \rightleftharpoons [\text{Ni}(\text{Dt}^0)_2]^{2+} + [\text{Ni}(\dot{\text{Dt}})_2] \tag{1}$$

$$2[\text{Ni}(\dot{\text{Dt}})(\ddot{\text{Dt}})]^- \rightleftharpoons [\text{Ni}(\dot{\text{Dt}})_2] + [\text{Ni}(\ddot{\text{Dt}})_2]^{2-} \tag{2}$$

$$\Delta G° = -RT(\ln K_c) = -nF(\Delta E) \tag{3}$$

The K_c values of for both processes, i.e., $(K_c)_1$ for eq 1 and $(K_c)_2$ for eq 2, respectively, are tabulated in Table 4. The large values of the K_c indicate that electron localized mixed-valence

Table 4. Calculated Comproportionality Constants at 298 K (^{n}Bu$_4$NClO$_4$ Supporting Electrolyte)

compound	$(K_c)_1$	$(K_c)_2$
[**1a**][BF$_4$]$_2$	1.18×10^5	2.80×10^5
[**1b**][BF$_4$]$_2$	7.20×10^4	1.30×10^5

species can be stabilized such that electrons are not redistributed between the two ligands. Interestingly, $(K_c)_1$ is 60 times larger in $[\mathbf{1a}][BF_4]_2$ than $[\mathbf{1b}][BF_4]_2$, indicating that such a mixed valence species would be more stable with isopropyl substitution on pyrazine nitrogen. It should also be noted that the calculated K_c values should be treated with caution as the change in solvent polarity and nature of electrolyte (use of noncoordinating electrolyte) can certainly change the observed redox potentials and thus K_c values.[102−104]

Electrochemical data of $[\mathbf{1a}][BF_4]_2$ and $[\mathbf{1b}][BF_4]_2$ clearly suggest electronic communications between the two non-innocent ligands. In order to obtain spectroscopic signatures of the reduced forms of these compounds, we have conducted a spectroelectrochemical investigation with the more soluble $[\mathbf{1a}][PF_6]$.[105] The results of the first reduction of $[\mathbf{1a}][PF_6]$ in acetonitrile and deuterated acetonitrile are very similar: a decrease of intensities of the bands at 542 and 610 nm as well as appearance of two new intense bands at 732 and 364 nm (Figure 5). In agreement with the electrochemical data, the
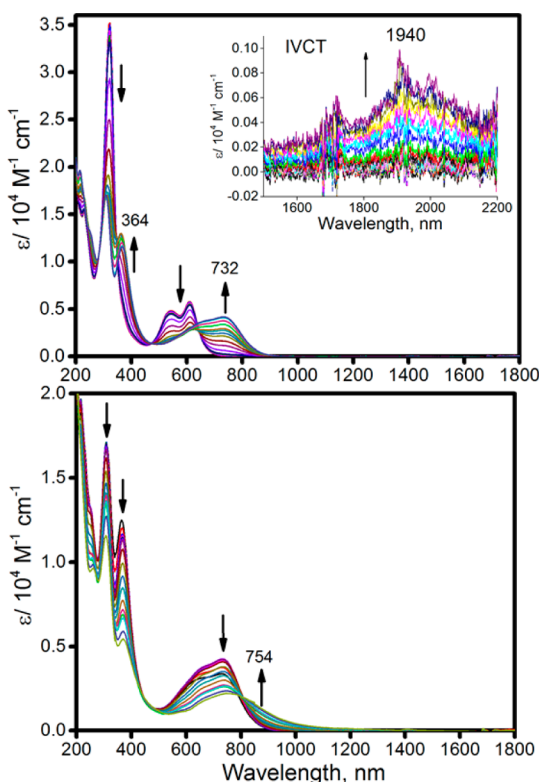

Figure 5. Electronic spectra of reduced $[\mathbf{1a}][PF_6]$, generated using spectroelectrochemistry (reduced in CD$_3$CN, see Experimental Section for details). Top: first reduction process. Bottom: second reduction process.

increase of the weak band at ∼1940 nm could be tentatively assigned to the intervalence charge transfer (IVCT) band and is consistent with the mixed-valence nature of the $[\mathbf{1a}]^+$ complex.[106,107] We also used band deconvolution analysis (Figure S6) to estimate an upper limit of the matrix coupling element H_{ab} in $[\mathbf{1a}]^+$ complex. Since an actual magnitude of the transition dipole moment for IVCT band is unknown, we used the shortest S−S interligand distance for such estimation and found that H_{ab} is ∼350 cm^{-1}. The magnitude of the H_{ab} is in the border of classical class II/III complexes. During the second reduction of the $[\mathbf{1a}]^+$ complex, an intensity of the band at 732

decreases, IVCT disappears, and a new broad band at 754 nm appears in the UV−vis spectrum of $[\mathbf{1a}]^0$.

IRMPD of $[\mathbf{1a}]^{2+}$ and $[\mathbf{2a}]^{2+}$. The IRMPD spectra generated from the discrete, gas phase $[\mathbf{1a}]^{2+}$ and $[\mathbf{2a}]^{2+}$ ions are shown, compared to predicted spectra based on DFT calculations, in Figure 6. Optimized structures are shown in Figure 7. Based on vibrational frequencies predicted by DFT, we are able to assign the IRMPD peaks to vibrational modes for both species.
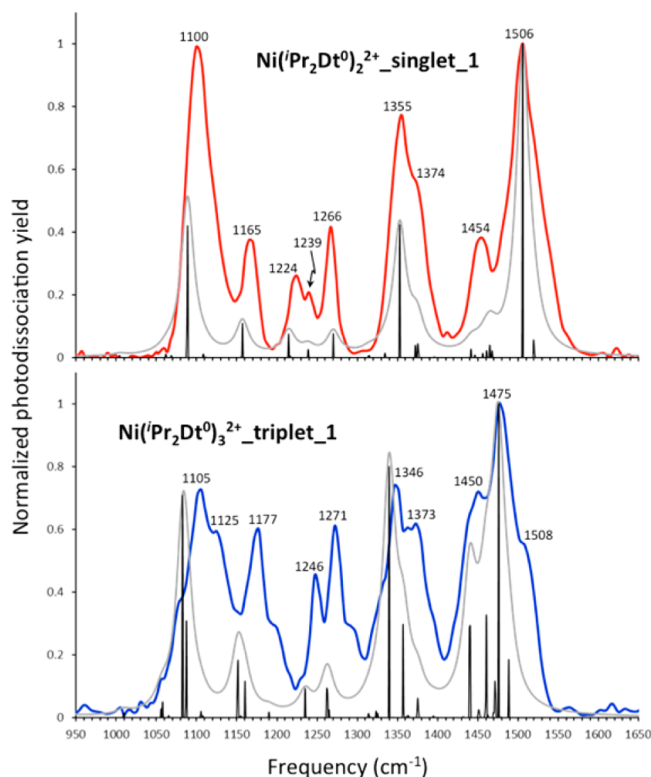

Figure 6. IRMPD spectra of gas phase $[\mathbf{1a}]^{2+}$ (top) and $[\mathbf{2a}]^{2+}$ (bottom) ions.

The prominent peak at 1506 cm^{-1}, in the region expected for imine −C═N− stretching, is assigned to symmetric stretching (with respect to the given dithione ligand) of the ring C═N bond (Table 5). A minor absorption corresponding to the asymmetric −C═N− stretching mode is predicted to appear at 1520 cm^{-1}. This peak is not resolved in the IRMPD spectrum, but may contribute to the shoulder to the high-frequency side of the absorption centered at 1506 cm^{-1}. The presence of C═N stretching suggests that in the gas phase the ligand exists, at least partially, in the dithiolato tautomeric form which is similar to the dizwitterionic character observed in the case of an oxo−molybdenum complex.[32] The absorption at 1454 cm^{-1} is assigned to a group of coupled −CH$_3$ scissor modes for the methyl groups of the isopropyl substituent of the ^{i}Pr$_2$Dt^0 ligand. DFT predicts 6 absorptions in this region, all of which involve the scissoring mode. However, in the IRMPD spectrum the peaks are not resolved. The absorption at 1355 cm^{-1} is assigned to stretching of the C═N bond coupled to rocking of the ring −CH$_2$− groups. The shoulder to the high-frequency side of the absorption appears to consist of two unresolved vibrations. One, predicted to appear at 1372 cm^{-1}, is the C−H bending mode of the isopropyl group. The other, predicted to appear at 1374 cm^{-1}, is a mode that involves the C−H bend and
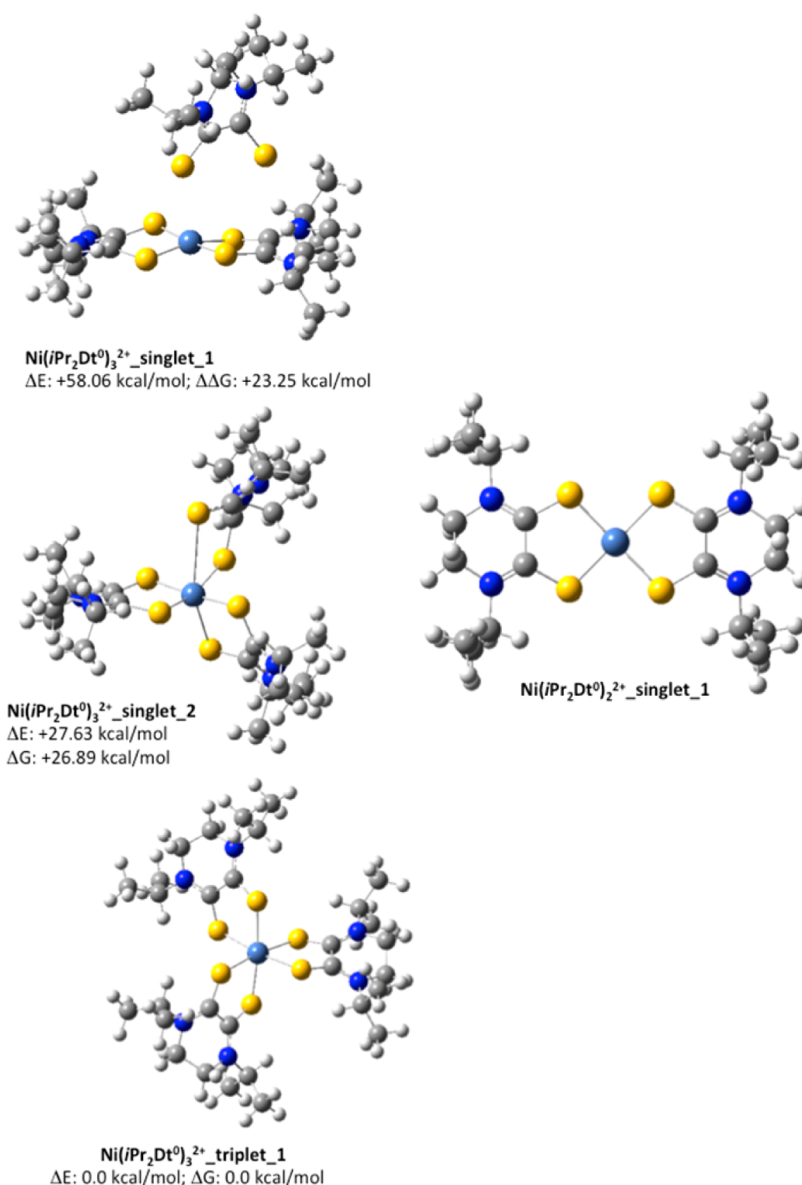
Ni(*i*Pr$_2$Dt^0)$_3$$^{2+}$_singlet_1
ΔE: +58.06 kcal/mol; ΔΔG: +23.25 kcal/mol

Ni(*i*Pr$_2$Dt^0)$_3$$^{2+}$_singlet_2
ΔE: +27.63 kcal/mol
ΔG: +26.89 kcal/mol

Ni(*i*Pr$_2$Dt^0)$_2$$^{2+}$_singlet_1

Ni(*i*Pr$_2$Dt^0)$_3$$^{2+}$_triplet_1
ΔE: 0.0 kcal/mol; ΔG: 0.0 kcal/mol

Figure 7. DFT predicted structures of [**1a**]$^{2+}$ and [**2a**]$^{2+}$.

Table 5. Observed (IRMPD) and Calculated (DFT) Vibrational Frequencies (in cm^{-1}) of [1a]$^{2+}$ along with Assignments

IRMPD	calcd scaled[a]	assignment
1506	1506	asym (ring) C=N stretch
1454	1441−1468	−CH$_3$ (*i*Pr) scissor modes
1375	1372, 1375	C−H (*i*Pr) bend, combination C−H (*i*Pr) and −CH$_3$ umbrella mode
1355	1353	coupled C=N stretch, ring CH$_2$−CH$_2$ rock
1267	1271	sym ring CH$_2$−CH$_2$ rock
1240	1239	coupled ring N−C−C bend, ring CH$_2$−CH$_2$ rock
1224	1218	coupled dithiolene C−C stretch, C−N−C(iPr) bend
1165	1158	coupled ring C−C=N bending
1100	1089	coupled dithiolene C−C stretch, ring breathing modes

[a]Calculated (at the B3LYP/6-311+G(d,p) level of theory) absorptions are scaled by a factor of 0.974.

symmetric bending (umbrella mode) of the methyl groups of the isopropyl group. Absorptions in the IRMPD spectra at 1239 and 1266 cm^{-1} are primarily assigned to other ring vibrations. The former is an N−C−C bending mode coupled to the ring −CH$_2$−CH$_2$− rock. The latter instead corresponds to the symmetric −CH$_2$−CH$_2$− rock. A third absorption involving primarily ring vibrations appears at 1165 cm^{-1} and is assigned to coupled C−C=N bending modes. The peak at 1224 cm^{-1} is assigned to the C−C stretch of the dithione group coupled to C−N−C(*i*Pr) bending motion. A second absorption featuring motion of the dithione C−C bond appears at 1100 cm^{-1}. This vibration also involves general "breathing" vibrations of the ring and isopropyl groups.

For Ni(*i*Pr$_2$Dt^0)$_3$$^{2+}$ (Figure 6), the absorptions attributed to C=N stretching are red-shifted to 1475 and 1508 cm^{-1}. The latter corresponds to the asymmetric stretching of the C=N groups within the *i*Pr$_2$Dt^0 ligands, and appears as a high-frequency shoulder. The shoulder at 1450 cm^{-1} corresponds to the −CH$_3$ bending modes of the isopropyl groups. The group of peaks from 1346 to 1373 cm^{-1} correspond to the C−H wag

of the isopropyl group (former), and the wag coupled to bending of the ring CH_2 groups and $C\equiv N$ stretching. The absorptions at 1246 and 1271 cm^{-1} are assigned to rocking motion of the ring CH_2 groups, while the peak at 1177 cm^{-1} corresponds to the ring C−N−C bending motions. Interestingly, DFT predicts that the C−C stretching modes of the dithione groups, those that make up the intense absorption at 1099 cm^{-1} for $[\mathbf{1a}]^{2+}$, are of extremely low intensity for $[\mathbf{2a}]^{2+}$ and should appear in the vicinity of 1110 cm^{-1}. The two poorly resolved peaks at 1125 and 1105 cm^{-1} instead can be assigned to ring C−C−N and C−N−C bending motions, with little coupling to C−C stretching of the dithione groups. Interestingly, all three calculated structures of $Ni(^iPr_2Dt^0)_3{}^{2+}$, i.e., two singlet and one triplet structure (Figure 7), have similar theoretical spectra. Coupled with the theoretical spectra, the resolution of the gas phase spectrum does not allow us to unambiguously assign the gas phase structures using IRMPD. However, DFT does predict the triplet structure to be lowest in energy consistent with the findings of more detailed electronic structure.

Electronic Structures of [1a]²⁺ and [2a]²⁺. Density functional theory (DFT) calculations were performed to understand the electronic structure $[\mathbf{1a}]^{2+}$ and $[\mathbf{2a}]^{2+}$. The molecular orbital energy diagram and representative shapes of frontier molecular orbitals predicted using the B3LYP exchange-correlation functional and Wachter's full-electron basis set for nickel and 6-311G(d) basis set for all other atoms are shown in Figures 8−11. The molecular orbital compositions are listed in Table 6.
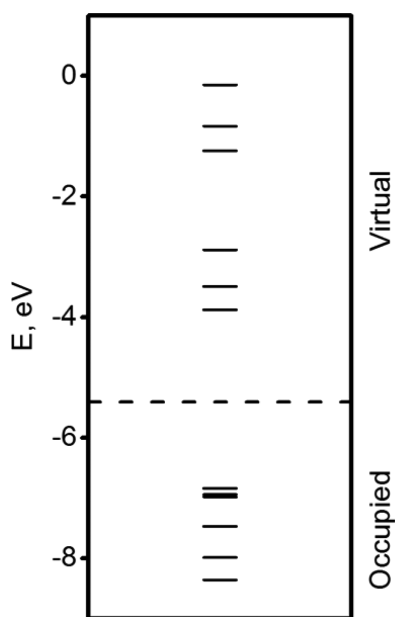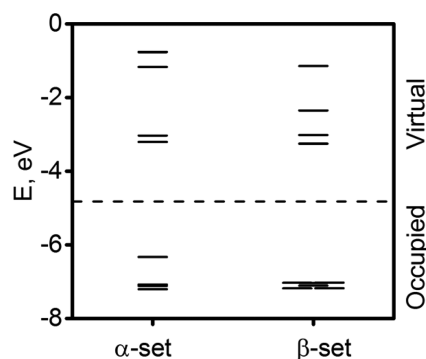

Figure 9. Molecular orbital diagrams of $[\mathbf{2a}]^{2+}$ calculated by DFT methodology using spin unrestricted formalism.
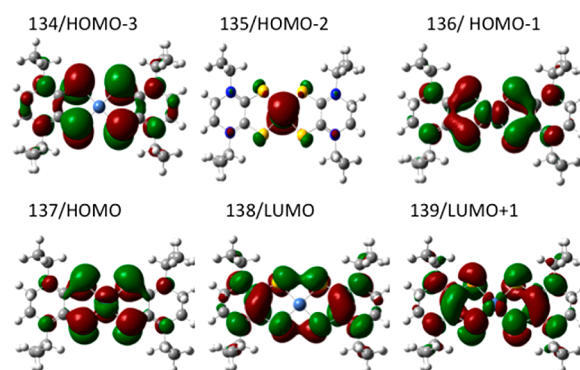

Figure 10. DFT predicted frontier molecular orbitals of $[\mathbf{1a}]^{2+}$.

MOs with a nickel d_{xy} character. The DFT-predicted LUMO (MO 138) in complex $[\mathbf{1a}]^{2+}$ is delocalized over two ligands with sulfur atom contribution of ∼19%, which is similar to the bis(dithiolene)Ni(II) complexes.[108] The nickel $d_{x^2−y^2}$ orbital contributes to LUMO+1 and LUMO+2, ∼7% and ∼24%, respectively. Overall, the DFT-predicted electronic structure of $[\mathbf{1a}]^{2+}$ supports ligand-centered reduction and is in agreement with experimental electrochemical data. It also suggests that metal-to-ligand charge transfer (MLCT) bands should dominate the low-energy region of the UV−vis spectrum in $[\mathbf{1a}]^{2+}$, while intraligand (IL) and predominantly nickel-centered d−d transitions appear at significantly higher energies. To test this assignment we have conducted TDDFT calculations on $[\mathbf{1a}]^{2+}$. TDDFT calculations allow correlating d−d, CT, and IL types of excited states with experimental UV−vis spectra of transition-metal compounds including those with thiolate or thione type ligands.[33,82,109] In agreement with the electronic structure calculations on complex $[\mathbf{1a}]^{2+}$, TDDFT predicts two major absorption regions in its UV−vis spectrum (Figure 12). The low energy region comprises 11 excited states and is dominated by MLCT character. Indeed, the 400−1000 nm region is dominated by the excited state 6, which corresponds to excitation from HOMO−1, with a large contribution from Ni d_{yz} AO, to LUMO (∼100% ligand). The energy and intensity of the transition to this excited state correlate well with the experimentally observed band at ∼540 nm (Figure 10). In addition, MLCT excited states 1−3 originating from predominantly nickel-centered HOMO − HOMO−2 to LUMO and LUMO+1 are predicted in this region. Although the TDDFT predicted intensities are very low (Supporting Information), they can borrow intensity from the second CT band, and thus be responsible for the first, low
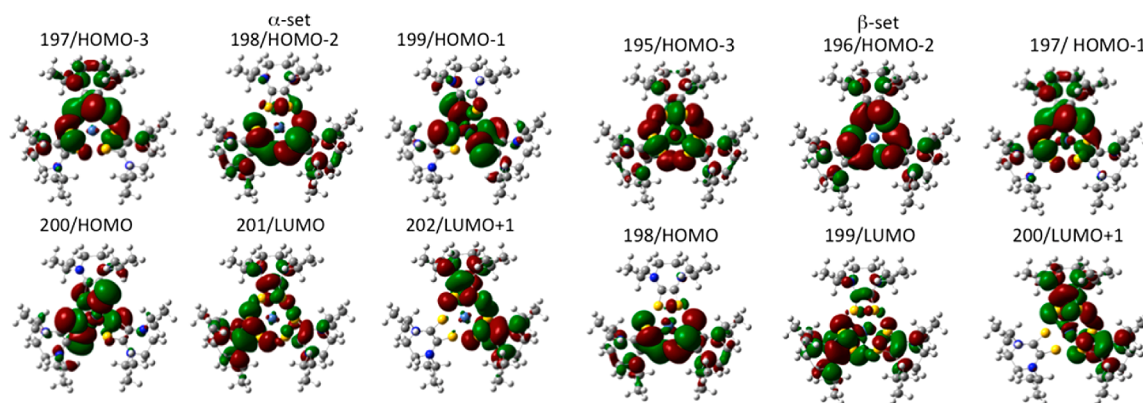

Figure 8. Molecular orbital diagrams of $[\mathbf{1a}]^{2+}$ calculated by DFT.

The electronic structure of $[\mathbf{1a}]^{2+}$ resembles a classic case of a d^8 Ni^{2+} ion in a square-planar environment. The molecular orbital composition diagram clearly shows four doubly occupied predominantly nickel-centered MOs in the HOMO region. The first three nickel-centered MOs are closely spaced in HOMO − HOMO−2 region and predominantly contain nickel d_{xz}, d_{yz}, and d_{z^2} character with the last two being nearly degenerate (Figure 8). These MOs are energetically separated by ∼0.5 eV from the rest of the occupied MOs, including the

Figure 11. DFT predicted frontier molecular orbitals of $[2a]^{2+}$.

Table 6. DFT Predicted Molecular Orbital Compositions for $[1a]^{2+}$ and $[2a]^{2+a}$

| MO	energy	% composition			
		Ni	S	N	C, H
		$[1a]^{2+}$			
132	−8.358	0.41	58.75	25.66	15.18
133	−7.988	1.47	84.62	0.5	13.41
134	−7.47	0	71.14	19.31	9.55
135	−6.983	89.92	7.07	1.35	1.65
136	−6.941	43.82	19.41	16	20.78
137	**-6.84**	**50.69**	**31.09**	**9.56**	**8.66**
138	**-3.878**	**0.18**	**18.65**	**33.01**	**48.16**
139	−3.493	6.74	26.38	22.49	44.38
140	−2.883	24.3	36.41	5.75	33.53
141	−1.238	3.89	22.33	13.94	59.84
142	−0.834	0.05	17.67	14.59	67.69
143	−0.147	29.25	22.54	0.46	47.75
		$[2a]^{2+}$, α-set			
195	−7.205	2.81	66.95	19.1	11.14
196	−7.112	0.21	58.49	28.4	12.9
197	−7.08	0.34	69.18	19.98	10.5
198	−7.076	0.35	69.16	20	10.49
199	−6.331	11.41	65.19	6.39	17
200	**-6.33**	**11.39**	**65.18**	**6.37**	**17.07**
201	**-3.207**	**0.37**	**24.44**	**26.66**	**48.54**
202	−3.206	0.37	24.36	26.68	48.59
203	−3.032	0.01	36.38	21.69	41.92
204	−1.168	7.1	22.98	13.35	56.57
205	−0.767	0.08	19.8	13.85	66.27
206	−0.759	0.08	19.7	13.82	66.4
		$[2a]^{2+}$, β-set			
193	−7.18	14.91	55.02	12.39	17.68
194	−7.178	14.93	55.13	12.39	17.55
195	−7.108	7.47	61.95	18.71	11.87
196	−7.035	0.35	62.79	25.13	11.72
197	−7.028	2.4	69.48	18.31	9.8
198	**-7.024**	**2.46**	**69.5**	**18.26**	**9.79**
199	**-3.255**	**3.03**	**23.78**	**26.98**	**46.21**
200	−3.251	2.98	23.73	26.99	46.3
201	−3.019	0.01	36.7	21.55	41.74
202	−2.352	40.97	20.62	8.45	29.96
203	−2.351	41.02	20.63	8.43	29.92
204	−1.143	6.37	23.2	13.46	56.97

^{a}HOMO and LUMO are in bold.
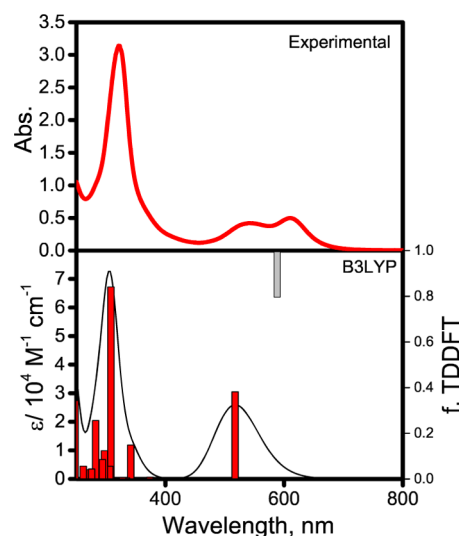
Figure 12. Experimental (top, $[1a][BF_4]_2$) and TDDFT predicted (bottom) UV−vis spectra of $[1a]^{2+}$. The energy of the TDDFT predicted most intense transition at ∼600 nm is shown with a gray vertical bar.

energy CT band observed at ∼630 nm in $[1a]^{2+}$ and $[1b]^{2+}$.[110−112] TDDFT also predicts that the most prominent absorption bands in the ∼350 nm region in $[1a]^{2+}$ (excited state 19) are IL in nature and originate from electron transfer from predominantly sulfur in- and out-of-plane occupied MOs to LUMO, LUMO+1, and LUMO+2.

In the case of $[2a]^{2+}$, simple ligand-field theory considerations for $O_h \rightarrow D_{3h} \rightarrow D_3$ symmetry descent predict e ($d_{x^2−y^2}$, d_{xy}) < a$_1$ (d_{z^2}) < e (d_{xz}, d_{yz}) or a$_1$ (d_{z^2}) < e ($d_{x^2−y^2}$, d_{xy}) < e (d_{xz}, d_{yz}) energy order. This energy ordering predicts that the d^8 Ni^{2+} electronic configuration in $[2a]^{2+}$ should result in a paramagnetic state. Accordingly, our DFT calculations support a triplet state as a ground state for $[2a]^{2+}$. Moreover, the experimentally observed ∼0.2 Å elongation of the Ni−S bonds in $[2a][BF_4]_2$ is also reproduced well by DFT calculations. Again, nickel-centered atomic orbitals contribute significantly to the SOMO and SOMO−1 region of α-set, and dominate the contribute into the SOMO−4 and SOMO−5 of the β-set. The low-energy unoccupied MOs are, again, predominantly ligand-centered. Similar to $[1a]^{2+}$, DFT predicted electronic structure of $[2a]^{2+}$ suggested that the first reduction should be ligand-centered; while the first oxidation should occur at the nickel center, which was not observed under experimental conditions.

■ SUMMARY

How the electrons are partitioned and how they interact in transition metal complexes of noninnocent ligands remain a fascinating area in chemistry. Dithiolene ligands are prototype examples of ligand redox noninnocence as they can exhibit different redox states from fully reduced dithiolene (Dt^{2-}) state to two electron fully oxidized dithione (Dt^0) state. In this study, we have focused on Ni(II) complexes of fully oxidized dithiolene ligands. We have synthesized nickel complexes of two oxidized dithiolene ligands, Me_2Dt^0 and $^iPr_2Dt^0$. The solid state structure of $[\mathbf{1a}][BF_4]_2$ has been determined that exhibits a classic square planar geometry at the metal center. Methanolic solutions of complex $[\mathbf{1a}][PF_6]_2$ spontaneously convert to a highly unusual tris(dithione)Ni(II) complex, $[\mathbf{2a}][PF_6]_2$. The corresponding BF_4 salt, $[\mathbf{2a}][BF_4]_2$, has been structurally characterized. The metal coordination sphere is symmetric, and the packing reveals a wheel-like structure created by the ligand disposition. The bis(dithione)Ni(II) complexes, i.e., $[Ni(R_2Dt^0)_2][X]_2$ (R = Me, ^iPr; X = BF_4, PF_6) exhibit two strong low-energy bands near 600 nm. The DFT calculations reveal a high degree of ligand character in the HOMO and LUMO orbitals that leads to these strong charge transfer transitions. The electronic calculations on the $[\mathbf{2a}]^{2+}$ indicate a spin-triplet ground state, consistent with paramagnetically shifted resonances in NMR spectra. The complexes also exhibit four clearly defined one-electron ligand based reduction couples. The redox potentials are invariant as a function of electrolyte, but they depend on the nature of the ligand. From the reduction potentials, the comproportionation constants have been calculated that indicate the feasibility of generating mixed valence species. Consistent with the redox properties, spectroelectrochemical experiments with $[\mathbf{1a}][PF_6]_2$ exhibit a low-intensity, low-energy intervalence charge transfer (IVCT) band at ~2000 nm. Band deconvolution analysis provides an upper limit to the ligand-to-ligand interaction to be ~350 cm^{-1}, bordering class II/III mixed valence species under Robin−Day classification. The presence of ligand centered mixed valence species demonstrates interligand communication, a feature that may be useful in designing electronic materials. The gas phase vibrational spectra of $[\mathbf{1a}]^{2+}$ and $[\mathbf{2a}]^{2+}$ have been examined by IRMPD spectroscopy, and the observed bands have been assigned with the help of DFT calculations. The vibrational spectrum is consistent with a spin-triplet ground state of $[\mathbf{2a}]^{2+}$, although it could not be uniquely defined.

■ ASSOCIATED CONTENT

ⓢ Supporting Information

The Supporting Information is available free of charge on the ACS Publications website at DOI: 10.1021/acs.inorgchem.5b00531.

> Crystallographic data for $[\mathbf{2a}][BF_4]_2$ (CIF)
> (Crystallographic data for $[\mathbf{1a}][BF_4]_2$ (CIF)
> Figures showing conversion of $[Ni(^iPr_2Dt^0)_2][PF_6]_2$ to $[Ni(^iPr_2Dt^0)_3][PF_6]_2$, maps of atomic orbital contributions to the frontier molecular orbital in $[\mathbf{1a}]^{2+}$ and $[\mathbf{2a}]^{2+}$, TDDFT derived transitions, a Gaussian fitting of the IVCT band, and the IRMPD spectra of $[\mathbf{2a}]^{2+}$ and calculated absorptions using the singlet states; a table of TDDFT predicted excitation energies and oscillator strengths for $[\mathbf{1a}]^{2+}$; coordinates for the DFT optimized geometries (PDF)

■ AUTHOR INFORMATION

Corresponding Authors
*E-mail: Basu@duq.edu.
*E-mail: Vanstipdonkm@duq.edu.
*E-mail: vnemykin@d.umn.edu.

Notes
The authors declare no competing financial interest.

■ REFERENCES

(1) Davison, A.; Edelstein, N.; Holm, R. H.; Maki, A. H. *Inorg. Chem.* **1963**, *2*, 1227−1232.

(2) Shupack, S. I.; Billig, E.; Clark, R. J. H.; Williams, R.; Gray, H. B. *J. Am. Chem. Soc.* **1964**, *86*, 4594−4602.

(3) Schrauzer, G. N.; Mayweg, V. P. *J. Am. Chem. Soc.* **1965**, *87*, 3585−3592.

(4) Fabian, J.; Nakazumi, H.; Matsuoka, M. *Chem. Rev.* **1992**, *92*, 1197−1226.

(5) Oliver, S. N.; Kershaw, S. V.; Underhill, A. E.; Hill, C. A. S.; Charlton, A. *Nonlinear Opt.* **1995**, *10*, 87−99.

(6) Connelly, N. G.; Locke, J.; McCleverty, J. A. *Inorg. Chim. Acta* **1968**, *2*, 409−410.

(7) Bui, T.-T.; Garreau-de Bonneval, B.; Moineau-Chane Ching, K. I. *New J. Chem.* **2010**, *34*, 337−347.

(8) Lieffrig, J.; Jeannin, O.; Auban-Senzier, P.; Fourmigue, M. *Inorg. Chem.* **2012**, *51*, 7144−7152.

(9) Pilia, L.; Espa, D.; Barsella, A.; Fort, A.; Makedonas, C.; Marchio, L.; Mercuri, M. L.; Serpe, A.; Mitsopoulou, C. A.; Deplano, P. *Inorg. Chem.* **2011**, *50*, 10015−10027.

(10) Soras, G.; Psaroudakis, N.; Mousdis, G. A.; Manos, M. J.; Tasioulos, A. J.; Aloukos, P.; Couris, S.; Labeguerie, P.; Lipinski, J.; Avramopoulos, A.; Papadopoulos, M. G. *Chem. Phys.* **2010**, *372*, 33−45.

(11) Serrano-Andres, L.; Avramopoulos, A.; Li, J.; Labeguerie, P.; Begue, D.; Kelloe, V.; Papadopoulos, M. G. *J. Chem. Phys.* **2009**, *131*, 134312.

(12) Chen, C.-T.; Liao, S.-Y.; Lin, K.-J.; Lai, L.-L. *MRS Online Proc. Libr.* **1997**, *488*, 165−170.

(13) Theriot, L. J.; Ganguli, K. K.; Kavarnos, S.; Bernal, I. *J. Inorg. Nucl. Chem.* **1969**, *31*, 3133−3140.

(14) Mueller-Westerhoff, U. T.; Vance, B.; Yoon, D. I. *Tetrahedron* **1991**, *47*, 909−932.

(15) Hintsa, E. J.; Hartman, J. R.; Cooper, S. R. *J. Am. Chem. Soc.* **1983**, *105*, 3738−3739.

(16) Bigoli, F.; Cassoux, P.; Deplano, P.; Mercuri, M. L.; Pellinghelli, M. A.; Pintus, G.; Serpe, A.; Trogu, E. F. *Dalton* **2000**, 4639−4644.

(17) Marshall, K. L.; Jacobs, S. D. *Mol. Cryst. Liq. Cryst.* **1988**, *159*, 181−196.

(18) Kambe, T.; Sakamoto, R.; Hoshiko, K.; Takada, K.; Miyachi, M.; Ryu, J.-H.; Sasaki, S.; Kim, J.; Nakazato, K.; Takata, M.; Nishihara, H. *J. Am. Chem. Soc.* **2013**, *135*, 2462−2465.

(19) Wang, K.; Stiefel, E. I. *Science* **2001**, *291*, 106−109.

(20) Dang, L.; Shibl, M. F.; Yang, X.; Alak, A.; Harrison, D. J.; Fekl, U.; Brothers, E. N.; Hall, M. B. *J. Am. Chem. Soc.* **2012**, *134*, 4481−4484.

(21) Kato, R. *Chem. Rev.* **2004**, *104*, 5319−5346.

(22) Hoshino, N.; Yoshii, Y.; Aonuma, M.; Kubo, K.; Nakamura, T.; Akutagawa, T. *Inorg. Chem.* **2012**, *51*, 12968−12975.

(23) Grate, J. W.; Rose-Pehrsson, S.; Barger, W. R. *Langmuir* **1988**, *4*, 1293−1301.

(24) Tan, W. L.; Ji, W.; Zuo, J. L.; Bai, J. F.; You, X. Z.; Lim, J. H.; Yang, S. S.; Hagan, D. J.; Van Stryland, E. W. *Proc. SPIE* **1999**, *3899*, 475−482.

(25) Sproules, S.; Wieghardt, K. *Coord. Chem. Rev.* **2010**, *254*, 1358−1382.

(26) Kaim, W.; Schwederski, B. *Coord. Chem. Rev.* **2010**, *254*, 1580−1588.

(27) Ray, K.; Petrenko, T.; Wieghardt, K.; Neese, F. *Dalton Trans* **2007**, 1552−1566.

(28) Espa, D.; Pilia, L.; Marchiò, L.; Pizzotti, M.; Robertson, N.; Tessore, F.; Mercuri, M. L.; Serpe, A.; Deplano, P. *Dalton Trans* **2012**, *41*, 12106−12113.

(29) Bigoli, F.; Deplano, P.; Mercuri, M. L.; Pellinghelli, M. A.; Pilia, L.; Pintus, G.; Serpe, A.; Trogu, E. F. *Inorg. Chem.* **2002**, *41*, 5241−5248.

(30) Basu, P.; Nigam, A.; Mogesa, B.; Denti, S.; Nemykin, V. N. *Inorg. Chim. Acta* **2010**, *363*, 2857−2864.

(31) Perera, E.; Basu, P. *Dalton Trans* **2009**, 5023−5028.

(32) Mtei, R. P.; Perera, E.; Mogesa, B.; Stein, B.; Basu, P.; Kirk, M. L. *Eur. J. Inorg. Chem.* **2011**, *2011*, 5467−5470.

(33) Nemykin, V. N.; Olsen, J. G.; Perera, E.; Basu, P. *Inorg. Chem.* **2006**, *45*, 3557−3568.

(34) Sproules, S.; Weyhermueller, T.; Goddard, R.; Wieghardt, K. *Inorg. Chem.* **2011**, *50*, 12623−12631.

(35) Sproules, S.; Banerjee, P.; Weyhermuller, T.; Yan, Y.; Donahue, J. P.; Wieghardt, K. *Inorg. Chem.* **2011**, *50*, 7106−7122.

(36) Tenderholt, A. L.; Wang, J.-J.; Szilagyi, R. K.; Holm, R. H.; Hodgson, K. O.; Hedman, B.; Solomon, E. I. *J. Am. Chem. Soc.* **2010**, *132*, 8359−8371.

(37) Holm, R. H.; Solomon, E. I.; Majumdar, A.; Tenderholt, A. *Coord. Chem. Rev.* **2011**, *255*, 993−1015.

(38) Tenderholt, A. L.; Hodgson, K. O.; Hedman, B.; Holm, R. H.; Solomon, E. I. *Inorg. Chem.* **2012**, *51*, 3436−3442.

(39) Van Stipdonk, M. J.; Basu, P.; Dille, S.; Gibson, J. K.; Berden, G.; Oomens, J. *J. Phys. Chem. A* **2014**, *118*, 5407−5418.

(40) Guo, L.; Ellis, D. E.; Gubanova, O. V.; Hoffman, B. M. *MRS Online Proc. Libr.* **1995**, *393*, 137−142.

(41) *SADABS*, Bruker AXS Inc.: Madison, WI, 2001.

(42) Sheldrick, G. M. *Acta Cryst.* **2008**, *A64*, 112−122.

(43) Dain, R. P.; Gresham, G.; Groenewold, G. S.; Steill, J. D.; Oomens, J.; Van Stipdonk, M. J. *Rapid Commun. Mass Spectrom.* **2013**, *27*, 1867−1872.

(44) Groenewold, G. S.; van Stipdonk, M. J.; Oomens, J.; de Jong, W. A.; McIlwain, M. E. *Int. J. Mass Spectrom.* **2011**, *308*, 175−180.

(45) Dain, R. P.; Gresham, G.; Groenewold, G. S.; Steill, J. D.; Oomens, J.; van Stipdonk, M. J. *Rapid Commun. Mass Spectrom.* **2011**, *25*, 1837−1846.

(46) Groenewold, G. S.; de Jong, W. A.; Oomens, J.; Van Stipdonk, M. J. *J. Am. Soc. Mass Spectrom.* **2010**, *21*, 719−727.

(47) Groenewold, G. S.; Gianotto, A. K.; Cossel, K. C.; Van Stipdonk, M. J.; Moore, D. T.; Polfer, N.; Oomens, J.; de Jong, W. A.; Visscher, L. *J. Am. Chem. Soc.* **2006**, *128*, 4802−4813.

(48) Leavitt, C. M.; Gresham, G. L.; Benson, M. T.; Gaumet, J.-J.; Peterman, D. R.; Klaehn, J. R.; Moser, M.; Aubriet, F.; Van Stipdonk, M. J.; Groenewold, G. S. *Inorg. Chem.* **2008**, *47*, 3056−3064.

(49) Moore, D. T.; Oomens, J.; Eyler, J. R.; von Helden, G.; Meijer, G.; Dunbar, R. C. *J. Am. Chem. Soc.* **2005**, *127*, 7243−7254.

(50) Bagratashvili, V. N.; Letokhov, V. S.; Makarov, A. A.; Ryabov, E. A. *Multiple Photon Infrared Laser Photophysics and Photochemistry*; Harwood Academic Publishers: 1985; 530 pp.

(51) Oomens, J.; Tielens, A. G. G. M.; Sartakov, B. G.; von Helden, G.; Meijer, G. *Astrophys. J.* **2003**, *591*, 968−985.

(52) Frisch, M. J.; Trucks, G. W.; Schlegel, H. B.; Scuseria, G. E.; Robb, M. A.; Cheeseman, J. R.; Montgomery, J. A., Jr.; Vreven, T.; Kudin, K. N.; Burant, J. C.; Millam, J. M.; Iyengar, S. S.; Tomasi, J.; Barone, V.; Mennucci, B.; Cossi, M.; Scalmani, G.; Rega, N.; Petersson, G. A.; Nakatsuji, H.; Hada, M.; Ehara, M.; Toyota, K.; Fukuda, R.; Hasegawa, J.; Ishida, M.; Nakajima, T.; Honda, Y.; Kitao, O.; Nakai, H.; Klene, M.; Li, X.; Knox, J. E.; Hratchian, H. P.; Cross, J. B.; Adamo, C.; Jaramillo, J.; Gomperts, R.; Stratmann, R. E.; Yazyev, O.; Austin, A. J.; Cammi, R.; Pomelli, C.; Ochterski, J. W.; Ayala, P. Y.; Morokuma, K.; Voth, G. A.; Salvador, P.; Dannenberg, J. J.; Zakrzewski, V. G.; Dapprich, S.; Daniels, A. D.; Strain, M. C.; Farkas, O.; Malick, D. K.; Rabuck, A. D.; Raghavachari, K.; Foresman, J. B.; Ortiz, J. V.; Cui, Q.; Baboul, A. G.; Clifford, S.; Cioslowski, J.; Stefanov, B. B.; Liu, G.; Liashenko, A.; Piskorz, P.; Komaromi, I.; Martin, R. L.; Fox, D. J.; Keith, T.; Al-Laham, M. A.; Peng, C. Y.; Nanayakkara, A.; Challacombe, M.; Gill, P. M. W.; Johnson, B.; Chen, W.; Wong, M. W.; Gonzalez, C.; Pople, J. A. *Gaussian 03, Revision C.02*; Gaussian, Inc.: Wallingford, CT, 2004.

(53) Nemykin, V. N.; Basu, P. *VMOdes Program, Revision A 7.2*; University of Minnesota Duluth and Duquesne University: 2005.

(54) Becke, A. D. *Phys. Rev. A: At., Mol., Opt. Phys.* **1988**, *38*, 3098−3100.

(55) Perdew, J. P. *Phys. Rev. B: Condens. Matter Mater. Phys.* **1986**, *33*, 8822−8824.

(56) Tao, J.; Perdew, J. P.; Staroverov, V. N.; Scuseria, G. E. *Phys. Rev. Lett.* **2003**, *91*, 146401.

(57) Becke, A. D. *J. Chem. Phys.* **1993**, *98*, 5648−5652.

(58) Nemykin, V. N.; Hadt, R. G.; Belosludov, R. V.; Mizuseki, H.; Kawazoe, Y. *J. Phys. Chem. A* **2007**, *111*, 12901−12913.

(59) Wachters, A. J. H. *J. Chem. Phys.* **1970**, *52*, 1033.

(60) McLean, A. D.; Chandler, G. S. *J. Chem. Phys.* **1980**, *72*, 5639−5648.

(61) Tomasi, J.; Mennucci, B.; Cammi, R. *Chem. Rev. (Washington, DC, U. S.)* **2005**, *105*, 2999−3093.

(62) Schlaepfer, C. W.; Nakamoto, K. *Inorg. Chem.* **1975**, *14*, 1338−1344.

(63) Wootton, J. L.; Zink, J. I. *J. Phys. Chem.* **1995**, *99*, 7251−7257.

(64) Kutsumizu, S.; Kojima, N.; Ban, T.; Tsujikawa, I. *Bull. Chem. Soc. Jpn.* **1987**, *60*, 2547−2553.

(65) Bigoli, F.; Deplano, P.; Mercuri, M. L.; Pellinghelli, M. A.; Pintus, G.; Serpe, A.; Trogu, E. F. *J. Am. Chem. Soc.* **2001**, *123*, 1788−1789.

(66) Bigoli, F.; Chen, C.-T.; Wu, W.-C.; Deplano, P.; Mercuri, M. L.; Pellinghelli, M. A.; Pilia, L.; Pintus, G.; Serpe, A.; Trogu, E. F. *Chem. Commun.* **2001**, 2246−2247.

(67) Matsubayashi, G.; Akiba, K.; Tanaka, T. *Inorg. Chim. Acta* **1989**, *157*, 195−199.

(68) Antolini, L.; Fabretti, A. C.; Franchini, G.; Menabue, L.; Pellacani, G. C.; Desseyn, H. O.; Dommisse, R.; Hofmans, H. C. *J. Chem. Soc., Dalton Trans.* **1987**, 1921−1928.

(69) Kato, R.; Mori, T.; Kobayashi, A.; Sasaki, Y.; Kobayashi, H. *Chem. Lett.* **1984**, 1−4.

(70) Khare, G. P.; Eisenberg, R. *Inorg. Chem.* **1970**, *9*, 2211−2217.

(71) Rae, A. I. M. *Chem. Commun.* **1967**, 1245−1246.

(72) Cooper, S. R.; Rawle, S. C.; Hartman, J. R.; Hintsa, E. J.; Admans, G. A. *Inorg. Chem.* **1988**, *27*, 1209−1214.

(73) Thorne, C. M.; Rawle, S. C.; Admans, G. A.; Cooper, S. R. *Inorg. Chem.* **1986**, *25*, 3848−3850.

(74) Bigoli, F.; Deplano, P.; Devillanova, F. A.; Ferraro, J. R.; Lippolis, V.; Lukes, P. J.; Mercuri, M. L.; Pellinghelli, M. A.; Trogu, E. F.; Williams, J. M. *Inorg. Chem.* **1997**, *36*, 1218−1226.

(75) Nomura, M.; Cauchy, T.; Geoffroy, M.; Adkine, P.; Fourmigue, M. *Inorg. Chem.* **2006**, *45*, 8194−8204.

(76) Waters, T.; Woo, H.-K.; Wang, X.-B.; Wang, L.-S. *J. Am. Chem. Soc.* **2006**, *128*, 4282−4291.

(77) Liu, S.-G.; Liu, Y.-Q.; Zhu, D.-B. *Synth. Met.* **1997**, *89*, 187−191.

(78) Bolligarla, R.; Durgaprasad, G.; Das, S. K. *Inorg. Chem. Commun.* **2011**, *14*, 809−813.

(79) Mines, T. E.; Geiger, W. E., Jr. *Inorg. Chem.* **1973**, *12*, 1189−1191.

(80) Geiger, W. E., Jr.; Mines, T. E.; Senftleber, F. C. *Inorg. Chem.* **1975**, *14*, 2141−2147.

(81) Kail, B.; Nemykin, V. N.; Davie, S. R.; Carrano, C. J.; Hammes, B.; Basu, P. *Inorg. Chem.* **2002**, *41*, 1281−1291.

(82) Basu, P.; Nemykin, V. N.; Sengar, R. S. *Inorg. Chem.* **2003**, *42*, 7489−7501.

(83) Sharma, A. K.; Kim, N.; Cameron, C. S.; Lyndon, M.; Gorman, C. B. *Inorg. Chem.* **2010**, *49*, 5072−5078.

(84) Cardona, C. M.; Mendoza, S.; Kaifer, A. E. *Chem. Soc. Rev.* **2000**, *29*, 37−42.

(85) Weyermann, P.; Gisselbrecht, J.-P.; Boudon, C.; Diederich, F.; Gross, M. *Angew. Chem., Int. Ed.* **1999**, *38*, 3215−3219.

(86) McNaughton, R. L.; Mondal, S.; Nemykin, V. N.; Basu, P.; Kirk, M. L. *Inorg. Chem.* **2005**, *44*, 8216−8222.

(87) Mondal, S.; Basu, P. *Inorg. Chem.* **2001**, *40*, 192−193.

(88) Sengar, R. S.; Basu, P. *Inorg. Chim. Acta* **2007**, *360*, 2092−2099.

(89) Ward, M. D. *Chem. Soc. Rev.* **1995**, *24*, 121−134.

(90) Hankache, J.; Wenger, O. S. *Chem. Rev.* **2011**, *111*, 5138−5178.

(91) Kaim, W.; Sarkar, B. *Coord. Chem. Rev.* **2013**, *257*, 1650−1659.

(92) Thomas, J. A. *Coord. Chem. Rev.* **2013**, *257*, 1555−1563.

(93) Kaim, W.; Lahiri, G. K. *Angew. Chem., Int. Ed.* **2007**, *46*, 1778−1796.

(94) Basu, P.; Enemark, J. H. *Inorg. Chim. Acta* **1997**, *263*, 81−85.

(95) Tom, G. M.; Creutz, C.; Taube, H. *J. Am. Chem. Soc.* **1974**, *96*, 7827−7828.

(96) Robin, M. B.; Day, P. *Adv. Inorg. Chem. Radiochem.* **1968**, *10*, 247−422.

(97) Li, X.-Y.; Sun, Y.-G.; Huo, P.; Shao, M.-Y.; Ji, S.-F.; Zhu, Q.-Y.; Dai, J. *Phys. Chem. Chem. Phys.* **2013**, *15*, 4016−4023.

(98) Jeannin, O.; Delaunay, J.; Barriere, F.; Fourmigue, M. *Inorg. Chem.* **2005**, *44*, 9763−9770.

(99) Szilagyi, R. K.; Lim, B. S.; Glaser, T.; Holm, R. H.; Hedman, B.; Hodgson, K. O.; Solomon, E. I. *J. Am. Chem. Soc.* **2003**, *125*, 9158−9169.

(100) Eisenberg, R.; Gray, H. B. *Inorg. Chem.* **2011**, *50*, 9741−9751.

(101) Basu, P.; Choudhury, S. B.; Pal, S.; Chakravorty, A. *Inorg. Chem.* **1989**, *28*, 2680−2686.

(102) D'Alessandro, D. M.; Keene, F. R. *Chem. Soc. Rev.* **2006**, *35*, 424−440.

(103) D'Alessandro, D. M.; Keene, F. R. *Dalton Trans* **2004**, 3950−3954.

(104) Goetsch, W. R.; Solntsev, P. V.; Van Stappen, C.; Purchel, A. A.; Dudkin, S. V.; Nemykin, V. N. *Organometallics* **2014**, *33*, 145−157.

(105) Following a reviewer's suggestion, the complex was reduced by bulk coulometry (Pt mesh working electrode, Pt auxiliary electrode, and Ag/AgCl reference electrode, in acetonitrile) under an Ar atmosphere; the odd electron species was detected by EPR spectroscopy at 77 K. A very weak axial spectrum ($g \sim 2.0036$, and 2.0025) was detected as the majority of the complex was oxidized during the sample transfer to the EPR tubes. Additional experiments are needed to fully understand the spectra.

(106) Nemykin, V. N.; Rohde, G. T.; Barrett, C. D.; Hadt, R. G.; Bizzarri, C.; Galloni, P.; Floris, B.; Nowik, I.; Herber, R. H.; Marrani, A. G.; Zanoni, R.; Loim, N. M. *J. Am. Chem. Soc.* **2009**, *131*, 14969−14978.

(107) Kubiak, C. P. *Inorg. Chem.* **2013**, *52*, 5663−5676.

(108) Bersuker, I. B. *Electronic Structure and Properties of Transition Metal Compounds: Introduction to the Theory*; John Wiley and Sons: 1996.

(109) Dammer, S. J.; Solntsev, P. V.; Sabin, J. R.; Nemykin, V. N. *Inorg. Chem.* **2013**, *52*, 9496−9510.

(110) Ray, K.; DeBeer George, S.; Solomon, E. I.; Wieghardt, K.; Neese, F. *Chem. - Eur. J.* **2007**, *13*, 2783−2797.

(111) Espa, D.; Pilia, L.; Marchio, L.; Mercuri, M. L.; Serpe, A.; Barsella, A.; Fort, A.; Dalgleish, S. J.; Robertson, N.; Deplano, P. *Inorg. Chem.* **2011**, *50*, 2058−2060.

(112) Pilia, L.; Espa, D.; Barsella, A.; Fort, A.; Makedonas, C.; Marchio, L.; Mercuri, M. L.; Serpe, A.; Mitsopoulou, C. A.; Deplano, P. *Inorg. Chem.* **2011**, *50*, 10015−10027.